

# Urban influence on the concentration and composition of submicron particulate matter in central Amazonia

Suzane S. de Sá (1), Brett B. Palm (2), Pedro Campuzano-Jost (2), Douglas A. Day (2), Weiwei Hu (2), Gabriel Isaacman-VanWertz<sup>a</sup> (3), Lindsay D. Yee (3), Joel Brito<sup>b</sup> (4), Samara Carbone<sup>c</sup> (4), Igor O. Ribeiro (5), Glauber G. Cirino<sup>d</sup> (6), Yingjun J. Liu<sup>e</sup> (1), Ryan Thalman<sup>f</sup> (7), Arthur Sedlacek (7), Aaron Funk (8), Courtney Schumacher (8), John E. Shilling (9), Johannes Schneider (10), Paulo Artaxo (4), Allen H. Goldstein (3), Rodrigo A.F. Souza (5), Jian Wang (7), Karena A. McKinney<sup>g</sup> (1), Henrique Barbosa (4), M. Lizabeth Alexander (11), Jose L. Jimenez (2), Scot T. Martin\* (1, 12)

- (1) School of Engineering and Applied Sciences, Harvard University, Cambridge, Massachusetts, USA
  - (2) Department of Chemistry and Cooperative Institute for Research in Environmental Sciences, University of Colorado, Boulder, Colorado, USA
  - (3) Department of Environmental Science, Policy, and Management, University of California, Berkeley, California, USA
  - (4) Institute of Physics, University of São Paulo, São Paulo, Brazil
  - (5) School of Technology, Amazonas State University, Manaus, Amazonas, Brazil
  - (6) National Institute for Amazonian Research, Manaus, Amazonas, Brazil
  - (7) Brookhaven National Laboratory, Upton, New York, USA
  - (8) Department of Atmospheric Sciences, Texas A&M University, College Station, Texas, USA
  - (9) Atmospheric Sciences and Global Change Division, Pacific Northwest National Laboratory, Richland, WA, USA
  - (10) Particle Chemistry Department, Max Planck Institute for Chemistry, Mainz, Germany
  - (11) Environmental Molecular Sciences Laboratory, Pacific Northwest National Laboratory, Richland, Washington, USA
  - (12) Department of Earth and Planetary Sciences, Harvard University, Cambridge, Massachusetts, USA
- <sup>a</sup> Now at Department of Civil and Environmental Engineering, Virginia Tech, Blacksburg, Virginia, USA  
<sup>b</sup> Now at Laboratory for Meteorological Physics (LaMP), University Blaise Pascal, Aubière, France  
<sup>c</sup> Now at Federal University of Uberlândia, Uberlândia, Minas Gerais, Brazil  
<sup>d</sup> Now at Department of Meteorology, Geosciences Institute, Federal University of Pará, Belém, Brazil  
<sup>e</sup> Now at University of California, Berkeley, California, USA  
<sup>f</sup> Now at Department of Chemistry, Snow College, Richfield, Utah, USA  
<sup>g</sup> Now at Colby College, Waterville, Maine, USA

Submitted: February 2018

*Atmospheric Chemistry and Physics*

\*To Whom Correspondence Should be Addressed

*E-mail: [scot\\_martin@harvard.edu](mailto:scot_martin@harvard.edu)*

*<https://martin.seas.harvard.edu/>*

1 **Abstract**

2           Fundamental to quantifying the influence of human activities on climate and air quality is  
3 an understanding of how anthropogenic emissions affect the concentrations and composition of  
4 airborne particulate matter (PM). The central Amazon basin, especially around the city of  
5 Manaus, Brazil, has experienced rapid changes in the past decades due to ongoing urbanization.  
6 Herein, changes in the concentration and composition of submicron PM due to pollution  
7 downwind of the Manaus metropolitan region are reported as part of the GoAmazon2014/5  
8 experiment. A high-resolution time-of-flight aerosol mass spectrometer (HR-ToF-AMS) and a  
9 suite of other gas- and particle-phase instruments were deployed at the “T3” research site, 70 km  
10 downwind of Manaus, during the wet season. At this site, organic components represented on  
11 average  $79 \pm 7\%$  of the non-refractory  $PM_{10}$  mass concentration, which was in the same range as  
12 several upwind sites. The organic  $PM_{10}$  was, however, considerably more oxidized at T3  
13 compared to upwind measurements. Positive-matrix factorization (PMF) was applied to the time  
14 series of organic mass spectra collected at the T3 site, yielding three factors representing  
15 secondary processes ( $73 \pm 15\%$  of total organic mass concentration) and three factors  
16 representing primary anthropogenic emissions ( $27 \pm 15\%$ ). Fuzzy c-means clustering (FCM) was  
17 applied to the afternoon time series of concentrations of  $NO_y$ , ozone, total particle number, black  
18 carbon, and sulfate. Four clusters were identified and characterized by distinct air mass origins  
19 and particle compositions. Two clusters, Bkgd-1 and Bkgd-2, were associated with background  
20 conditions. Bkgd-1 appeared to represent near-field atmospheric PM production and oxidation of  
21 a day or less. Bkgd-2 appeared to represent material transported and oxidized for two or more  
22 days, often with out-of-basin contributions. Two other clusters, Pol-1 and Pol-2, represented the  
23 Manaus influence, one apparently associated with the northern region of Manaus and the other

24 with the southern region of the city. A composite of the PMF and FCM analyses provided  
25 insights into the anthropogenic effects on PM concentration and composition. The increase in  
26 mass concentration of submicron PM ranged from 25% to 200% under polluted compared to  
27 background conditions, including contributions from both primary and secondary PM.  
28 Furthermore, a comparison of PMF factor loadings for different clusters suggested a shift in the  
29 pathways of PM production under polluted conditions. Nitrogen oxides may have played a  
30 critical role in these shifts. Increased concentrations of nitrogen oxides can shift pathways of PM  
31 production from HO<sub>2</sub>-dominant to NO-dominant as well as increase the concentrations of  
32 oxidants in the atmosphere. Consequently, the oxidation of biogenic and anthropogenic precursor  
33 gases as well as the oxidative processing of pre-existing atmospheric PM can be accelerated. The  
34 combined set of results demonstrates the susceptibility of atmospheric chemistry, air quality, and  
35 associated climate forcing to anthropogenic perturbations over tropical forests.

## 1 **1. Introduction**

2           Secondary organic material (SOM) constitutes a large fraction of the atmospheric particle  
3 burden (Hallquist et al., 2009; Jimenez et al., 2009) and therefore has important effects on the  
4 Earth's radiation balance, atmospheric visibility, and human health. SOM is a complex mixture  
5 of compounds resulting from many chemical pathways, and the processes underlying the  
6 production of SOM remain poorly understood. Models are especially challenged to accurately  
7 represent production of SOM in regions where there is a mix of biogenic and anthropogenic  
8 emissions (de Gouw et al., 2008; Glasius and Goldstein, 2016; Shrivastava et al., 2017). Possible  
9 shifts in the contributing mechanisms of SOM production between background and polluted  
10 conditions must be understood and quantified for distinct environments on the globe to test and  
11 enable accurate modeling predictions.

12           Several field observations, mainly in mid-latitudes of the Northern Hemisphere, and  
13 modeling efforts have suggested that the production of SOM from biogenic precursor  
14 compounds becomes more efficient in polluted air (Weber et al., 2007; Goldstein et al., 2009;  
15 Hoyle et al., 2011; Huang et al., 2014; Zhang et al., 2018). In the northeastern USA, de Gouw et  
16 al. (2005) showed that concentrations of organic particulate matter (PM) correlated well with  
17 anthropogenic tracers, yet the concentrations of the anthropogenic precursors were insufficient to  
18 explain the observed PM concentrations. In the southeastern USA, radioisotope analysis of  
19 organic PM determined that 70% to 80% of the carbon mass had a modern origin even as  
20 correlations were observed between SOM mass concentrations and anthropogenic VOC and CO  
21 concentrations (Weber et al., 2007). This finding and those of further field studies in the region  
22 together suggested that the organic PM was produced mainly from biogenic VOCs (BVOCs) yet  
23 modulated by anthropogenic emissions of NO<sub>x</sub> and SO<sub>2</sub> (Hu et al., 2015; Xu et al., 2015a; Xu et

24 al., 2015b; Zhang et al., 2018). In the western USA, ground and aircraft measurements observed  
25 the highest organic PM increases when air masses having high BVOC concentrations intercepted  
26 anthropogenic emissions (Setyan et al., 2012; Shilling et al., 2013). A metastudy for several  
27 locations in the USA concluded that air downwind of urban areas had increased organic PM  
28 concentrations due to the photochemical production of SOM (De Gouw and Jimenez, 2009).  
29 Models have estimated that 50% to 70% of the biogenic SOM mass concentration in several  
30 locations is modulated by anthropogenic emissions (Carlton et al., 2010; Heald et al., 2011;  
31 Spracklen et al., 2011). In addition, global-scale modeling studies have estimated an increase of  
32 20% to 60% in the global annual mean SOM concentration relative to the pre-industrial period  
33 (Tsigaridis et al., 2006; Hoyle et al., 2009).

34 Many possible mechanisms may contribute to the effects of anthropogenic emissions on  
35 increased SOM production, including changes in gas-particle partitioning, new particle  
36 production and growth, and particle acidity. Changes in the concentrations of nitrogen oxides,  
37 however, should be regarded as a critical factor (Hoyle et al., 2011 and references therein).  
38 Different NO<sub>x</sub> regimes favor distinct gas-phase oxidation pathways, leading to different  
39 oxidation products and particle yields, as evidenced in isoprene photo-oxidation (Kroll et al.,  
40 2005, 2006; Hallquist et al., 2009; Worton et al., 2013; Liu et al., 2016b; Liu et al., 2016a).  
41 Isoprene accounts for half of global BVOC mass emissions, and tropical forests are responsible  
42 for about 80% of terpenoid emissions (Guenther et al., 2012). In the Amazon, isoprene is the  
43 dominant BVOC emitted by vegetation and is estimated to contribute to about half of the organic  
44 PM concentrations under background conditions (Kuhn et al., 2010; Chen et al., 2015; Yáñez-  
45 Serrano et al., 2015). Under HO<sub>2</sub>-dominant conditions (i.e., low NO<sub>x</sub>), isoprene epoxydiols  
46 (IEPOX) are produced in the gas phase and, through heterogenous reactions involving sulfate,

47 PM is produced (Paulot et al., 2009; Surratt et al., 2010). Depending on the relative importance  
48 of increased concentrations of sulfate and NO<sub>x</sub> associated with pollution in a given region, an  
49 enhancement or suppression of IEPOX-derived PM production relative to background conditions  
50 may occur (Xu et al., 2015a; de Sá et al., 2017). As part of GoAmazon2014/5, de Sá et al. (2017)  
51 demonstrated that PM derived from IEPOX generally decreased under polluted compared to  
52 background conditions downwind of Manaus. Nitrogen oxides in the pollution plume suppressed  
53 the production of isoprene hydroxyhydroperoxides (Liu et al., 2016b), leading to a decrease in  
54 the production of gas phase IEPOX and consequently of IEPOX-derived PM (de Sá et al., 2017).

55 Amazonia, the largest tropical forest in the world and a large global source of SOM, is  
56 comparatively understudied relative to northern mid-latitude regions, especially with respect to  
57 the influence of pollution on the SOM lifecycle (Martin et al., 2010a). Manaus, a city of over two  
58 million people in the central Amazon, continuously releases an urban plume into an otherwise  
59 mostly unperturbed region (Kuhn et al., 2010; Martin et al., 2017). The region downwind of  
60 Manaus, especially in the wet season in the absence of regional fires (Artaxo et al., 2013), offers  
61 a natural laboratory for the investigation of biogenic-anthropogenic interactions and the resulting  
62 consequences for the amount and composition of PM in the region.

63 The present study investigates the influences of urban pollution on the concentration and  
64 composition of fine particles in central Amazonia, focusing on organic PM and its several  
65 component classes. The analysis employs data sets collected in the wet season from February 1  
66 to March 31, 2014, corresponding to the first Intensive Operating Period (IOP1) of the  
67 GoAmazon2014/5 experiment (Martin et al., 2016). Herein, positive-matrix factorization (PMF)  
68 of organic mass spectra measured by aerosol mass spectrometry (AMS) in conjunction with a  
69 clustering analysis of pollution indicators by Fuzzy c-means are employed to investigate the

70 changes in particle concentration and composition associated with the influence of urban  
71 pollution downwind of Manaus.

## 72 **2. Methodology**

### 73 **2.1 Site description**

74 The primary site of this study, named “T3” (3.2133 °S, 60.5987 °W), was located 70 km  
75 to the west of Manaus, Brazil, in central Amazonia (Martin et al., 2016). The site was situated in  
76 a pasture of 2.5 km × 2 km surrounded by forest. Based on modeled flow trajectories of the  
77 pollution plume, the T3 site intercepted the plume about 40% of the time (Martin et al., 2017).  
78 Auxiliary sites “T0a” and “T0t”, served as references for background conditions in relation to T3  
79 (Figure S1). Site T0a (2.1466 °S, 59.0050 °W) refers to the Amazonian Tall Tower Observatory  
80 (ATTO; Andreae et al., 2015), located 150 km to the northeast of Manaus. Site T0t (2.5946°S,  
81 60.2093°W) was situated 60 km to the north-northwest of Manaus in the Cuieiras Biological  
82 Reserve (“ZF2”) and refers to tower “TT34”, established in 2008 for the AMAZE-08 experiment  
83 (Martin et al., 2010b). The T0 sites were typically upwind of Manaus, with only occasional  
84 transport of pollution to these sites (Andreae et al., 2015; Chen et al., 2015). Auxiliary site “T2”  
85 served as a reference for polluted conditions. This site was located just across the Rio Negro  
86 (3.1392°S, 60.1315°W), 8 km from the southwestern edge of Manaus and typically downwind of  
87 urban emissions during the daytime.

### 88 **2.2 Aerosol Mass Spectrometry**

89 Characterization of the atmospheric PM was obtained using a High-Resolution Time-of-  
90 Flight Aerosol Mass Spectrometer (hereafter AMS; Aerodyne, Inc., Billerica, Massachusetts,  
91 USA; DeCarlo et al., 2006; Canagaratna et al., 2007). Detailed aspects of the AMS operation in  
92 GoAmazon2014/5 were presented in de Sá et al. (2017). In brief, the instrument was housed

93 within a temperature-controlled research container, and the inlet to the instrument sampled from  
94 5 m above ground level. Ambient measurements for this study were obtained every other 4 min.  
95 The other 4 min were used for analysis of output from an oxidation flow reactor as presented in  
96 Palm et al. (2018).

97 Data analysis was performed using *SQUIRREL* (1.56D) and *PIKA* (1.14G) of the AMS  
98 software suite (Sueper and collaborators; DeCarlo et al., 2006). Organic, sulfate, ammonium,  
99 nitrate, and chloride PM mass concentrations were quantified. “Sulfate” and “nitrate”  
100 concentrations reported by the AMS may include contributions from both organic and inorganic  
101 species (Farmer et al., 2010; Liao et al., 2015). Organic and inorganic nitrate concentrations were  
102 estimated based on the ratio of  $\text{NO}_2^+$  to  $\text{NO}^+$  signal intensity, as described in Section S2 (Fry et  
103 al., 2009; Farmer et al., 2010; Fry et al., 2013). The organic elemental ratios, O:C and H:C, were  
104 calculated following the methods of Canagaratna et al. (2015).

### 105 **2.3 Auxiliary measurements and datasets**

106 In complement to the AMS data set, the analysis herein incorporated auxiliary gas and  
107 particle measurements collected during IOP1 at T3 (Martin et al., 2016). Mass concentrations of  
108 molecular and tracer organic species in the gas and particle phases were measured by a Semi-  
109 Volatile Thermal Desorption Aerosol Gas Chromatograph (SV-TAG) at a time resolution of one  
110 hour (Isaacman-VanWertz et al., 2016). Concentrations of volatile organic compounds (VOCs)  
111 were measured by a Proton-Transfer-Reaction Time-of-Flight Mass Spectrometer (PTR-ToF-  
112 MS; Liu et al., 2016b). In the Mobile Aerosol Observing System (MAOS) of the ARM Climate  
113 Research Facility (ACRF; Martin et al., 2016), measurements of  $\text{NO}_y$  were made using a  
114 chemiluminescence-based instrument (Air Quality Design). The raw  $\text{NO}_y$  measurements (10-s  
115 resolution) were averaged across 30-min intervals to dampen the influence of brief local events.



116 In addition, ozone concentrations were measured by an ultraviolet photometric analyzer (Thermo  
117 Fisher, model 49i, Ozone Analyzer). Particle number concentrations were measured by a  
118 Condensation Particle Counter (TSI, model 3772). Black carbon (BC) concentrations were  
119 measured both by a 7-wavelength aethalometer (Magee Scientific, model AE-31) and a Single  
120 Particle Soot Photometer (SP2; Droplet Measurement Techniques). The two datasets differed by  
121 a factor of up to three in absolute mass concentrations, as observed in other studies (Subramanian  
122 et al., 2007; Cappa et al., 2008; Lack et al., 2008), but they agreed well in the temporal trend.  
123 The analysis herein for BC is thus restricted to the temporal trends. Wind direction, solar  
124 irradiance, and precipitation rate were measured by the ARM Mobile Facility (AMF-1), which  
125 was also part of the ACRF.

126 Additional measurements from T0a, T0t, and T2 were also used in the analysis. At T2,  
127 non-refractory particle composition and concentration were measured by an Aerosol Chemical  
128 Speciation Monitor (ACSM) during the wet season from March 9 to April 30, 2014 (Cirino et al.,  
129 submitted). ACSM measurements were made at T0a during the wet season of 2015, from  
130 February 1 to March 31 (Andreae et al., 2015). Further AMS datasets collected at T0t during the  
131 wet season of 2008 (February 6 to March 22; AMAZE-08 campaign) were used in the analysis  
132 (Chen et al., 2009; Schneider et al., 2011).

#### 133 **2.4 Air mass backtrajectories and precipitation rates**

134 Simulations of two-day backward air mass trajectories, starting at 100 m above T3, were  
135 made using HYSPLIT4 (Draxler and Hess, 1998). Input meteorological data were obtained  
136 from the Global Data Assimilation System (GDAS), provided by the NOAA Air Resources  
137 Laboratory (ARL), on a regular grid of  $0.5^\circ \times 0.5^\circ$ , 18 pressure levels, and 3-h intervals.  
138 Trajectory steps were calculated for every 12 min.

139 Information on precipitation along the trajectories was obtained from the S-band radar of  
140 the System for Amazon Protection (SIPAM) in Manaus (Machado et al., 2014). The radar had a  
141 beam width of  $1.8^\circ$ , and it scanned 17 elevation angles every 12 min. Data were recorded to a  
142 range of 240 km at 500-m gate spacing. The reflectivity fields were quality controlled to remove  
143 non-meteorological echo and calibrated against the satellite precipitation radar of the Tropical  
144 Rainfall Measuring Mission and Global Precipitation Measurement (TRMM-GPM; Kummerow  
145 et al., 1998; Hou et al., 2014). Ground clutter was used to analyze the stability of the calibration.  
146 The data were gridded at  $2 \text{ km} \times 2 \text{ km}$  in the horizontal and 0.5 km in the vertical using the  
147 NCAR *Radx* software. The reflectivity at 2.5 km in altitude was converted to rain rates based on  
148 the data sets of a Joss-Waldvogel disdrometer (Joss and Waldvogel, 1967), located at T3, 70 km  
149 downwind of the radar.

### 150 **3. Results and discussion**

#### 151 **3.1 Fine-mode PM composition**

152 The time series of mass concentrations of  $\text{PM}_1$  species at T3 during the wet season of  
153 2014 are plotted in Figure 1a. Organic material dominated the composition, contributing  $79 \pm 7\%$   
154 (average  $\pm$  one standard deviation), followed by sulfate ( $13 \pm 5\%$ ). The standard deviation  
155 quantifies the variability across the time series. Average non-refractory (NR)  $\text{PM}_1$  mass  
156 concentrations and compositions at T3 as well as at three other sites in the region are represented  
157 in Figure 1b. The two T0 sites corresponded to predominantly background conditions. By  
158 contrast, the T2 site represented conditions just downwind of Manaus, and depending on wind  
159 direction experienced fresh Manaus pollution or background air. The comparison in Figure 1b  
160 demonstrates that the organic component consistently constituted 70% to 80% of NR- $\text{PM}_1$  across

161 sites in this region in the wet season, for both background and polluted conditions, in line with  
162 previous observations (Chen et al., 2009; Martin et al., 2010a).

163 Even as the relative composition was similar across all sites, there were differences in the  
164 absolute mass concentrations (Figure 1b, top panel). The NR-PM<sub>1</sub> mass concentrations at the T0  
165 sites upwind of Manaus, although measured in different years, were consistently around 1 µg m<sup>-3</sup>  
166 <sup>3</sup>. The concentrations at the T2 site just downwind of Manaus were more than three times higher  
167 on average (3.3 µg m<sup>-3</sup>). Average concentrations at the T3 site (1.7 µg m<sup>-3</sup>), several hours  
168 downwind of Manaus, were lower compared to those at T2. This relative progression from T0, to  
169 T2, and then to T3 can be understood as a first-order quantification of the overall effect of  
170 Manaus emissions in increasing the airborne PM burden in the downwind region.

171 The diel trends of organic and sulfate mass concentrations as well as their variabilities  
172 across the four sites are shown in Figure 2. Lines represent means, solid markers show medians,  
173 and boxes span interquartile ranges. Organic mass concentrations and associated variability were  
174 higher at the T3 site compared to the T0 sites, markedly so in the afternoon hours. The greater  
175 variability at T3 is in line with a time-varying influence of Manaus emissions. This influence  
176 waxes and wanes with small northerly or southerly shifts of the trade winds as well as other  
177 changes in regional circulation tied to daily meteorology (dos Santos et al., 2014; Martin et al.,  
178 2017). The higher afternoon mass concentrations at T3 can be attributed to a combination of (i)  
179 an oxidant-rich, sunlight-fed plume that increases the production rate of secondary PM and (ii)  
180 faster near-surface winds during the day that transport PM from Manaus to T3 with less loss by  
181 deposition and dispersion compared to more-stagnant air at night. Among all sites, the T2  
182 observations had both the highest average organic mass concentrations and the largest  
183 variability. These characteristics of the T2 dataset can be explained by a combination of (i) the

184 proximity of the site to Manaus, (ii) the rapid and 180° changes in wind direction caused by the  
185 intersection of the trade winds with a local river breeze (dos Santos et al., 2014), and (iii)  
186 possible contributions of emissions from brick kilns, located mostly southwest of the site,  
187 especially during night time (Martin et al., 2016; Cirino et al., submitted).

188         The diel trends of the sulfate mass concentrations were in large part similar to those of  
189 the organic mass concentrations. One distinction in the case of sulfate, however, is that the  
190 variability at the T0 sites is similar to that at the T3 site. The explanation is that the background  
191 sources of sulfate, including not only in-basin emissions but also out-of-basin long-range  
192 transport, are variable and significant enough to make the variability at the background sites  
193 similar to that at the T3 site (de Sá et al., 2017).

194         Overall, the organic PM<sub>1</sub> at T3 was highly oxidized, as indicated by the position of gray  
195 markers in the plot of Figure 3. By contrast, the blue markers represent the dataset collected at  
196 T2 during the same period. The datasets encompass all times of days and all conditions at both  
197 sites. Datasets from background sites collected in different years are shown in Figure S2. Points  
198 to the upper left represent more oxidized material, and points to the lower right represent less  
199 oxidized material (Ng et al., 2011a). The comparison depicted in Figure 3 indicates the effects  
200 of the plume over the 4 h of transport from T2 to T3, which were investigated in detail by Cirino  
201 et al. (submitted). The plot suggests that the enhanced oxidative cycle associated with higher OH  
202 and O<sub>3</sub> concentrations in the pollution plume might cause (i) the production of highly oxidized  
203 SOM, from both biogenic and anthropogenic precursors including aromatic compounds  
204 (Chhabra et al., 2011; Lambe et al., 2011), and (ii) the accelerated oxidative processing of pre-  
205 existing organic PM by OH and O<sub>3</sub> (Martin et al., 2017). The implication is that the emissions

206 from Manaus can significantly affect the mechanisms that produce or modify fine-mode PM over  
207 the tropical forest.

### 208 **3.2 Characterization of organic PM by positive-matrix factorization**

209 Positive-matrix factorization was applied to the time series of the organic component of  
210 the high-resolution mass spectra (Ulbrich et al., 2009b). Diagnostics of the PMF analysis are  
211 presented in the Supplement (Section S1; Figures S3 and S4). Herein, “factor profile” and “factor  
212 loading” refer to the mathematical products of the multivariate statistical analysis, whereas  
213 “mass spectrum” and “mass concentration” refer to direct measurements.

214 A six-factor solution was obtained based both on the numerical diagnostics of the PMF  
215 algorithm and the judged scientific meaningfulness of the resolved factors (Section S1). The  
216 factor profiles, diel trends of the factor loadings, and the time series of the factor loadings and  
217 other related measurements are plotted in Figures 4a, 4b, and 4c, respectively. The inset of  
218 Figure 4a shows the mean fractional loading contribution of each factor during the analysis  
219 period. The correlations of factor loadings with co-located measurements of gas- and particle-  
220 phase species are shown in Figure 5.

221 The scientific interpretation of each factor was based on a combination of (i) the  
222 characteristics of the factor profile (i.e., “mass spectrum”), as referenced to a worldwide database  
223 of AMS spectra and PMF analyses (Ulbrich et al., 2009b; Ulbrich et al., 2009c, 2009a), and (ii)  
224 the temporal correlations between the factor loading and other co-located measurements (Figure  
225 5). Three factors interpreted as primary emissions of organic PM were resolved: an  
226 anthropogenic-dominated factor (hereafter, “ADOA”), a biomass burning factor (“BBOA”), and  
227 a fossil-fuel hydrocarbon-like factor (“HOA”). Three factors interpreted as secondary production  
228 and processing were resolved: a more-oxidized oxygenated factor (“MO-OOA”), a less-oxidized

229 oxygenated factor (“LO-OOA”), and an isoprene epoxydiols-derived factor (“IEPOX-SOA”).  
230 Figure 5 shows that the correlations of factor loadings with external measurements of gas- and  
231 particle-phase species support this interpretation, as detailed in the following discussion for each  
232 factor.

233         The HOA factor profile had characteristic ions of  $C_4H_7^+$  and  $C_4H_9^+$  at nominal values of  
234  $m/z$  55 and 57, respectively (Figure 4a). It had an oxygen-to-carbon (O:C) ratio of  $0.18 \pm 0.02$ ,  
235 the lowest among the six factors (Table 1). In line with the AMS PMF literature, the HOA factor  
236 represents a class of primary hydrocarbon-like organic compounds that are typically associated  
237 with traffic emissions (Zhang et al., 2005). In the present study, the HOA factor loadings  
238 accounted for 6% of the organic mass concentrations on average (Figure 4a, inset). As a point of  
239 comparison, the average in the southeastern USA typically varies from 9% to 15% (Xu et al.,  
240 2015b). The lower relative contribution of 6% in this study might in part be due to a larger  
241 relative role of secondary production in the environment of a tropical forest. In addition, the  
242 distance from Manaus to the T3 site might allow time for substantial vertical mixing, dilution,  
243 and subsequent evaporation of primary emissions into entrained background air (Robinson et al.,  
244 2007; Liu et al., accepted; Shilling et al., in preparation). Finally, the possible differences in  
245 emission profiles associated with different types of regional economic development between the  
246 Brazilian Amazon and the southeastern USA (e.g., fleet density, fuel matrix, industry, and so  
247 forth) should also be considered. The HOA factor loading decreased during the day, which can  
248 be explained by the growth of the planetary boundary layer (PBL) and the subsequent dilution of  
249 the concentrations of primary emissions (Figure 4b). The time series of HOA factor loading did  
250 not correlate well ( $R < 0.5$ ) with any of the co-located measurements at T3 (Figure 5). It is  
251 plotted alongside the time series of  $NO_y$  concentration in Figure 4c.

252 The BBOA factor profile was characterized by distinct peaks of  $C_2H_4O_2^+$  ( $m/z$  60) and  
253  $C_3H_5O_2^+$  ( $m/z$  73), as shown in Figure 4a. These peaks can be attributed to levoglucosan and  
254 other anhydrous sugars that result from biomass pyrolysis (Schneider et al., 2006; Cubison et al.,  
255 2011). Correlations of the factor loadings with the mass concentrations of levoglucosan and  
256 vanillin ( $R > 0.8$ ) measured by SV-TAG corroborate the association with biomass burning  
257 (Figure 4c; Figure 5). The BBOA factor of this study had an O:C ratio of  $0.61 \pm 0.08$  (Table 1),  
258 which is consistent with large contributions from levoglucosan (O:C of 0.83) and similar sugars.  
259 The factor loading on average accounted for 9% of the organic  $PM_1$  mass concentration (Figure  
260 4a, inset). This result is consistent with the low incidence of fires in the Amazon during the wet  
261 season (Martin et al., 2016). The BBOA factor loading typically decreased during the day  
262 (Figure 4b), which is suggestive of the dilution of local sources during the development of the  
263 PBL rather than long-range transport. Emissions from local fires around T3, including trash and  
264 tree burning, as well as from wood-fueled brick kilns along the road from Manaus to T3 might  
265 have contributed to this factor.

266 The ADOA factor profile, distinguished prominently by the  $C_7H_7^+$  ion at  $m/z$  91, also had  
267 characteristic ions of  $C_4H_7^+$  at  $m/z$  55 and  $C_3H_5^+$  at  $m/z$  41 (Figure 4a). A peak at  $m/z$  91 can  
268 arise from many sources, including biogenic and anthropogenic emissions (Ng et al., 2011b). In  
269 itself,  $m/z$  91 therefore does not serve as a tracer for a specific source or process without  
270 consideration of the atmospheric context. Factors having a characteristic  $m/z$  91 peak (usually  
271 labeled “91fac”) typically have been associated with biogenic emissions (Robinson et al., 2011;  
272 Budisulistiorini et al., 2015; Chen et al., 2015; Riva et al., 2016). The ADOA factor profile of  
273 this study, however, more strongly resembles the mass spectra previously reported for PM  
274 emissions from cooking activities (Lanz et al., 2007; Mohr et al., 2012) than those from “91fac”

275 (Section S1; Figure S5). The ratio of  $m/z$  55 to  $m/z$  57 of the ADOA factor was 4.1. This ratio  
276 lies in the range of 2 to 10 reported for several factors representing primary cooking emissions  
277 and is well above the range of 0.8 to 1.4 reported for factors associated with traffic emissions,  
278 i.e., HOA (Mohr et al., 2012 and references therein; Hu et al., 2016). Even though the ADOA  
279 factor profile has a large contribution from non-oxygenated ions, similar to the HOA factor and  
280 consistent with a dominance by primary emissions, it also contains considerable signal from  
281 oxygenated ions, resulting in a relatively higher O:C of  $0.40 \pm 0.05$  (Table 1). The factor loading  
282 on average accounted for 13% of the organic  $PM_{10}$  mass concentration (Figure 4a, inset). The  
283 factor loading decreased as the PBL developed during the day, consistent with dominant non-  
284 photochemical, primary sources (Figure 4b). Furthermore, there were increases, albeit small, in  
285 factor loading at 12:00 and 18:00 (local time), suggestive of breakfast-time and lunch-time  
286 cooking activities in Manaus based on a transport time of 4 to 6 h between the city and the T3  
287 site (Martin et al., 2016; Cirino et al., submitted). Manaus typically has four rush-hour periods  
288 each day from 6:30 to 8:00, 12:00 to 13:30, 16:30 to 18:30, and 21:00 to 22:00. Traffic peaking  
289 at these hours may therefore also have contributed to the ADOA factor. Correlations between  
290 factor loading and external measurements exceeded  $R = 0.5$  for many anthropogenic markers,  
291 including concentrations of aromatics (e.g., benzene, toluene, and  $C_8$  and  $C_9$  species), carbon  
292 monoxide, particle count, and  $NO_y$  (Figure 4c, Figure 5). Contributions from secondary  
293 processes cannot be ruled out, and it is possible that PM production from anthropogenic VOCs  
294 might have also been captured in this factor. Overall, the ADOA factor was interpreted in the  
295 present study as an indicator of anthropogenic influence associated with several sources in  
296 Manaus, most importantly cooking and possibly traffic emissions.



297 The IEPOX-SOA factor profile had marker ions of  $C_4H_5^+$  ( $m/z$  53) and  $C_5H_6O^+$  ( $m/z$  82)  
298 (Figure 4a; Lin et al., 2012; Hu et al., 2015; de Sá et al., 2017). It had an O:C ratio of  $0.9 \pm 0.10$   
299 (Table 1). The factor loading on average accounted for 17% of the organic  $PM_1$  mass  
300 concentration (Figure 4a, inset). There were high correlations ( $R > 0.8$ ) between factor loadings  
301 and concentrations of  $C_5$ -alkenetriols and 2-methyltetrols, which are markers of IEPOX-derived  
302 PM, produced by the photo-oxidation of isoprene under  $HO_2$ -dominant conditions (Surratt et al.,  
303 2010; Lin et al., 2012; Figure 4c). The increase in factor loading during daytime was consistent  
304 with a photochemical source (Figure 4b). There were also correlations between factor loadings  
305 and concentrations of sulfate and some acids, such as tricarballic acid (TCA; Figure 5), in  
306 agreement with the association of IEPOX-derived PM and sulfate/acidity observed in other  
307 studies (Budisulistiorini et al., 2013; Nguyen et al., 2014; Kuwata et al., 2015). Overall, this  
308 factor was therefore interpreted as representative of PM produced from isoprene photo-oxidation  
309 under  $HO_2$ -dominant conditions. The effects of urban pollution on the loadings of this factor  
310 were the focus of a previous publication (de Sá et al., 2017).

311 The two remaining factors, LO-OOA and MO-OOA, were also associated with secondary  
312 atmospheric processes. The LO-OOA and MO-OOA factors had O:C ratios of  $0.72 \pm 0.10$  and  
313  $1.09 \pm 0.17$ , respectively. The LO-OOA factor was characterized by the greatest ratio of signal  
314 intensity of the  $C_2H_3O^+$  ion ( $m/z$  43) to that of the  $CO_2^+$  ion ( $m/z$  44) (Figure 4a) compared to all  
315 other factors. This factor is usually attributed to lower-generation, less-oxidized, higher-volatility  
316 secondary organic PM (Jimenez et al., 2009). By comparison, the MO-OOA factor profile had  
317 the strongest  $CO_2^+$  ( $m/z$  44) peak among all factors (Figure 4a). This factor is usually attributed  
318 to higher-generation, more-oxidized, less-volatile secondary organic PM or extensively oxidized

319 primary PM of any type that has resided in the atmosphere for several days or more (Jimenez et  
320 al., 2009).

321 The LO-OOA factor loading on average accounted for 25% of the organic PM<sub>1</sub> mass  
322 concentration (Figure 4a, inset). The factor loading correlated better with the estimated  
323 concentrations of inorganic nitrate than with organic or total nitrate (Figure 5; Section S2 and  
324 Figure S6), which is consistent with the interpretation of the higher volatility associated with this  
325 factor (Jimenez et al., 2009; Zhang et al., 2011). The factor loading also correlated ( $R > 0.7$ ) with  
326 the concentrations of 2-methylglyceric acid and methyl-butyl-tricarboxylic acid (MBTCA),  
327 which are products of isoprene and monoterpene oxidation, respectively, under NO-dominant  
328 conditions (Figure 4c; Figure 5). The factor loading increased starting at 9:00 (local time) and  
329 peaked in the afternoon hours (Figure 4b). This diel trend, tied to the sunlight cycle, tracked the  
330 typical daily emission patterns of isoprene and monoterpenes from the surrounding forest  
331 (Yáñez-Serrano et al., 2015). The absence of a sharp decline at sunset and the higher variability  
332 at nighttime may also indicate a contribution by terpene ozonolysis. For these several reasons,  
333 the LO-OOA factor was interpreted herein as secondary organic PM produced mostly within  
334 several hours of observations by many possible pathways, including (i) the photo-oxidation of  
335 isoprene along non-IEPOX pathways, (ii) the photo-oxidation of terpenes and other biogenic  
336 VOCs along both HO<sub>2</sub>- and NO-dominant reaction pathways, (iii) the ozonolysis of terpenes,  
337 and (iv) the possible production of SOM from anthropogenic emissions from Manaus.

338 The MO-OOA factor loading on average accounted for 30% of the organic PM<sub>1</sub> mass  
339 concentration (Figure 4a, inset). The factor loading correlated ( $R > 0.7$ ) with the mass  
340 concentrations of several particle-phase carboxylic acids as well as the concentrations of sulfate,  
341 ammonium, and ozone (Figure 5). The time series of malic acid and ozone concentrations are

342 shown alongside the MO-OOA factor loadings in Figure 4c. Malic acid is a highly oxidized  
343 compound (O:C of 1.25), which may have many different sources (Röhrl and Lammel, 2002; van  
344 Pinxteren et al., 2014). The MO-OOA factor loading increased starting at 8:00 (local time;  
345 sunrise was at 6:00) and peaked between 10:00 and 16:00, with a large variability in the factor  
346 loadings in the afternoon hours among different days (Figure 4b). The afternoon increase and  
347 day-to-day variability were consistent with strong but variable photochemical processing leading  
348 to further oxidation of organic PM during the day, depending on daily weather. The high O:C of  
349  $1.09 \pm 0.17$  could also be indicative of production of PM from aromatic compounds emitted from  
350 Manaus (Chhabra et al., 2011; Lambe et al., 2011). Overall, this factor was interpreted to  
351 represent highly oxidized PM from multiple processes. Species initially associated with HOA,  
352 BBOA, ADOA, IEPOX-SOA, and LO-OOA factors may converge after sufficient atmospheric  
353 oxidation to become represented by the MO-OOA factor (Jimenez et al., 2009; Palm et al.,  
354 2018).

### 355 **3.3 Shifts in PM with anthropogenic influences**

#### 356 **3.3.1 Cluster Analysis**

357 To further investigate changes in the concentration and composition of PM associated  
358 with anthropogenic influences, a Fuzzy c-means (FCM) algorithm was applied to the time series  
359 of concentrations of particle number,  $\text{NO}_y$ , ozone, black carbon, and sulfate measurements at the  
360 T3 site (Bezdek et al., 1984). The analysis was fully independent of the PMF results. For each  
361 point in time, these concentrations represented the spatial coordinates of the data point. As  
362 discussed below, four clusters were identified. Based on measures of spatial similarity, the  
363 clustering algorithm attributed to each data point a degree of membership relative to each of the  
364 four clusters (Section S3; Figure S7 and Figure S8).

365 The scope of the clustering analysis was restricted to afternoon time points for which ten-  
366 hour air mass backtrajectories did not intersect significant precipitation and for which solar  
367 irradiance at T3 averaged over the previous 4 h was higher than  $200 \text{ W m}^{-2}$  (Section S3). This  
368 scope aimed at capturing fair-weather conditions and thereby minimizing the role of otherwise  
369 confounding processes, such as boundary layer dynamics and wet deposition. The elimination of  
370 trajectories having precipitation, however, should not be regarded as fully accurate given the  
371 uncertainties in the HYSPLIT trajectories. The scoped dataset spanned 24 afternoons.

372 Four clusters were identified based on minimization of the FCM objective function as  
373 well as a subjective assessment of meaningful interpretation of the set of clusters (Section S3).  
374 The FCM algorithm returned a matrix containing the degrees of membership (ranging from 0 to  
375 1) to each of the four clusters (columns) for each point in time (rows). For any given time point  
376 (i.e., row), the sum of its degrees of membership to clusters (i.e., sum across columns) was  
377 always unity, by definition. A collection of examples, representing 37% of the analyzed data  
378 points by FCM, is shown in Figure 6a. For times predominantly associated with only one cluster  
379 (e.g., Feb 9 and Feb 10), the corresponding air mass backtrajectories are plotted in Figure 7. The  
380 FCM algorithm also returned the coordinates of cluster centroids, which are listed in Table 2.

381 Two clusters of data were interpreted as “background” and labeled “Bkgd-1” and “Bkgd-  
382 2”. They were characterized by  $\text{NO}_y < 1 \text{ ppb}$ , ozone  $< 20 \text{ ppb}$ , and particle number  $< 1200 \text{ cm}^{-3}$   
383 (Table 2; Figure 6). The two clusters differed especially in that Bkgd-2 had significantly larger  
384 concentrations of sulfate and black carbon. A comparison of the datasets of Feb 13  
385 (predominantly Bkgd-1) and Feb 16 (predominantly Bkgd-2) in Figure 6 highlights these  
386 differences. Concentrations of sulfate and black carbon were  $0.15$  and  $0.10 \mu\text{g m}^{-3}$ , respectively,  
387 on Feb 13, compared to  $0.40$  and  $0.15 \mu\text{g m}^{-3}$  on Feb 16. The backtrajectories associated with

388 Bkgd-1 had both northeasterly and southeasterly components. The wind fields, out of line with  
389 the trade winds, may suggest passage through recent weather systems and may imply wet  
390 deposition, which in turn might explain lower gas and particle concentrations (Table 2). These  
391 recent weather systems might not have been excluded from the scoped dataset because of  
392 inaccuracies in the intersections of the backtrajectories with precipitation data, as discussed  
393 above, or because they were more distant than captured by the 10-h backtrajectories. Consistent  
394 with this hypothesis, the centroid value calculated for the 4-h averaged solar irradiance at T3  
395 (Section 3.3.2) was lower for Bkgd-1 ( $400 \text{ W m}^{-2}$ ) compared to the other clusters ( $600 \text{ W m}^{-2}$ ),  
396 suggesting an association of Bkgd-1 with overcast conditions. By comparison, the  
397 backtrajectories associated with Bkgd-2 were predominantly from the northeast, coming from the  
398 direction of the T0t and T0a sites (Figure 7), in line with the dominant trade winds of the wet  
399 season. The air masses of Bkgd-2 may have experienced less wet deposition and may represent  
400 more extensive atmospheric oxidation than those of Bkgd-1. They may also have carried PM  
401 contributions from out-of-basin sources, which would be consistent with the higher sulfate and  
402 black carbon concentrations of Bkgd-2 compared to Bkgd-1 (Chen et al., 2009; Pöhlker et al.,  
403 2017).

404 Two other clusters were interpreted as “polluted” and labeled “Pol-1” and “Pol-2”. They  
405 were characterized by concentrations of  $\text{NO}_y > 1 \text{ ppb}$ , ozone  $> 20 \text{ ppb}$ , and particle number  $>$   
406  $1200 \text{ cm}^{-3}$  (Table 2; Figure 6). The dataset of the afternoon of Mar 9 illustrates a shift in  
407 dominance from Pol-2 to Pol-1 (Figure 6). Although Pol-1 and Pol-2 both have high  
408 concentrations of sulfate and other pollutants, they differ in the extent of those high  
409 concentrations. The explanation may be that these clusters represent different source regions.  
410 Pol-1 may be associated with emissions from the northern region of Manaus, and Pol-2 may be

411 associated with emissions from the southern region of Manaus. Industry, power production, and  
412 oil refineries are concentrated in the southeastern region of Manaus (Figure S9; Medeiros et al.,  
413 2017). Population density and commercial activity is concentrated in the southwestern portion of  
414 the city where downtown is located (Figure S10). Aircraft observations show that concentrations  
415 of sulfate as well as other pollutants are higher in the urban outflow from the southern compared  
416 to the northern region of Manaus (Figure S10). Directional plots of SO<sub>2</sub> and particle number  
417 concentrations observed at the T2 site further demonstrate the heterogeneity in Manaus  
418 emissions (Figure S10). This hypothesis of a geographical difference in source regions  
419 qualitatively aligns with the differences in backtrajectories characteristic of times dominated by  
420 Pol-1 and Pol-2 (Figure 7). This interpretation does imply, however, that the backtrajectories  
421 may have a 20° inaccuracy. Such inaccuracy is reasonable for the application of HYSPLIT  
422 modeling in this region given (i) the absence of surface weather stations and (ii) the relatively  
423 large scale of input wind fields (i.e., 50 km) compared to the scale of modeling (i.e., 70 km from  
424 T3 to Manaus and a city cross section of 20 km).

### 425 **3.3.2 Comparison of PM among clusters**

426 The characteristic PM composition associated with each cluster was determined by  
427 calculating the centroid coordinates of the clusters for the AMS species and PMF factors  
428 (Section S3). The centroid coordinate of a cluster for a given variable is defined as a weighted  
429 mean of that variable across all points in time, where the weight is the degree of membership of  
430 each data point to that cluster. A comparison of PM<sub>1</sub> concentrations and compositions for the  
431 four clusters is shown in Figure 8. Values are listed in Table 2.

432 The NR-PM<sub>1</sub> mass concentrations increased by 25% to 200% in clusters Pol-1 and Pol-2  
433 compared to clusters Bkgd-1 and Bkgd-2 (Figure 8a). Increases in sulfate and associated

434 ammonium concentrations had a smaller yet non-negligible role in the increased PM<sub>1</sub> mass  
435 concentrations. Sources of sulfate other than Manaus sustain relatively high concentrations in the  
436 Amazon basin, as represented by the Bkgd-2 cluster (Chen et al., 2009; de Sá et al., 2017).  
437 Compared to these regional background concentrations (i.e., Bkgd-2 cluster), the increases in  
438 sulfate concentrations were significant only for air masses associated with the heavily  
439 industrialized and densely populated southern region of Manaus (i.e., Pol-2 cluster).

440         With respect to the composition of the organic PM, Figure 8b shows that the Bkgd-1  
441 cluster had large contribution from the LO-OOA factor. By comparison, the Bkgd-2 cluster had  
442 larger contributions from the MO-OOA and IEPOX-SOA factors. A comparison of 13 Feb and  
443 16 Feb of 2014 (Figure 6d) illustrates these findings. The low mass concentrations and the  
444 dominant contribution by the LO-OOA factor suggest that the Bkgd-1 cluster may represent  
445 conditions under which secondary organic PM was produced within recent hours through photo-  
446 oxidation of VOCs emitted by the forest and subsequent condensation of secondary organic  
447 material. The low sulfate concentrations for Bkgd-1 may rationalize the absence of a significant  
448 contribution by the IEPOX-SOA factor. Isoprene photo-oxidation may have contributed to PM  
449 production by pathways other than IEPOX uptake (Krechmer et al., 2015; Riva et al., 2016). By  
450 comparison, for Bkgd-2, the higher mass concentrations and the greater contributions by IEPOX-  
451 SOA and MO-OOA factors suggest that this cluster may represent conditions under which  
452 secondary organic PM was a combination of material produced both on that day as well as on  
453 previous days. During transport, the organic PM may have undergone extensive atmospheric  
454 oxidation by a combination of surface and condensed-phase chemistry, including cloud water  
455 processes (Carlton et al., 2006; Ervens et al., 2011; Hoyle et al., 2011; Perraud et al., 2012).

456 Concentrations and composition of the Bkgd-2 cluster may therefore represent an extensive  
457 geographical footprint.

458 The organic PM concentration and composition associated with the Pol-1 and Pol-2  
459 clusters were distinct from those of the Bkgd-1 and Bkgd-2 clusters (Figure 8). The mass  
460 concentrations of organic PM were greater by 25% to 150% for Pol-1 and Pol-2. According to  
461 the PMF factors (Figure 8b), the larger part of this increase in organic PM between the  
462 background and polluted clusters was tied to the production of secondary organic PM, although  
463 primary emissions also contributed significantly. By comparison, for both Bkgd-1 and Bkgd-2  
464 clusters, contributions by primary emissions were negligible, as indicated by the low summed  
465 contribution of factors of primary origin (i.e., ADOA, BBOA, and HOA) to the organic PM<sub>1</sub> (<  
466 10%). For Pol-1 and Pol-2, the ADOA factor loading on average accounted for 10% of the  
467 organic mass concentration at T3, serving as a strong marker of Manaus pollution. A comparison  
468 of February 9 and March 9 with February 13 and 16 illustrates these findings (Figure 6d).

469 In regard to secondary organic PM, the IEPOX-SOA factor loading decreased by almost  
470 50% under polluted compared to background conditions. de Sá et al. (2017) attributed this  
471 decrease to the suppression of IEPOX production by elevated NO concentrations. This  
472 suppression typically outweighed possible enhancements in IEPOX uptake and subsequent PM  
473 production because of elevated sulfate concentrations. By contrast, the LO-OOA and MO-OOA  
474 factor loadings increased by 50% to 100% under polluted conditions. These increases exceeded  
475 the decrease in IEPOX-SOA factor loadings, resulting in a net increase of around 100% in mass  
476 concentration of secondary organic PM (Figure 8).

477 The shifts in the processes governing the production of secondary organic PM because of  
478 increased NO<sub>x</sub>, OH, and O<sub>3</sub> concentrations characteristic of the pollution plume were complex



479 and non-linear (Figure 9a). Overall, the oxidation pathways were driven faster. The relatively  
480 high  $f_{\text{CO}_2^+}$  values and O:C ratios of all factors (Table 1), including those associated with primary  
481 emissions, compared to typical values at other locations worldwide (Canagaratna et al., 2015),  
482 corroborate this interpretation. Ozone concentrations in the plume increase by 200% to 300%,  
483 and hydroxyl radical concentrations increased by 250% or more (Liu et al., accepted). As HO<sub>2</sub>-  
484 dominant pathways were inhibited, NO-dominant pathways became active. Increased oxidant  
485 concentrations may also have promoted additional multigenerational chemistry of semi- or  
486 intermediate-volatility species (Robinson et al., 2007). Oxidation of VOCs by aqueous-phase  
487 reactions, including in-cloud processing, and oxidation of biomass burning emissions may also  
488 have played roles to varying degrees on different days (Carlton et al., 2006; Ervens et al., 2011;  
489 Hoyle et al., 2011; Perraud et al., 2012). In addition, when primary and secondary PM mass  
490 concentrations increased, further uptake of oxidized semi-volatile molecules could have been  
491 thermodynamically favored according to partitioning theory, representing a positive feedback on  
492 the increase of mass concentrations (Pankow, 1994; Odum et al., 1996; Carlton et al., 2010).

493         The increase in the LO-OOA and MO-OOA factor loadings associated with Pol-1 and  
494 Pol-2 indicates that the net effect of this accelerated and modified chemistry was the quick  
495 production and further oxidation of secondary organic PM. Precursors may have included both  
496 the wide range of biogenic VOCs as well as contributions from anthropogenic precursors, such  
497 as gas-phase species from vehicle emissions or evaporated primary material (Nordin et al., 2013;  
498 Presto et al., 2014). The LO-OOA factor loading was important for the polluted conditions of  
499 Pol-1 and Pol-2 as well as for the clean conditions of Bkgd-1. This result is not necessarily  
500 because of an in-common molecular composition but rather because of an in-common process,  
501 i.e., fresh production of secondary organic PM (Figure 9b). Likewise, the MO-OOA factor

502 loading was important for Pol-1, Pol-2, and Bkgd-2 because this factor represented an in-  
503 common process, i.e., extensive oxidation (Figure 9b). In the case of the MO-OOA factor, there  
504 is also an overall in-common composition characterized by highly oxidized species even as  
505 precursor species and subsequent oxidation pathways differed (Jimenez et al., 2009).

506         The complexity of the real atmospheric processes, as illustrated in Figure 9, is to some  
507 extent captured by the instrumental and analytical tools herein employed. Positive-matrix  
508 factorization identified several broad classes of organic PM. Some PMF factors had sufficiently  
509 unique signatures that they could be associated to one specific source and/or process (e.g., HOA  
510 and IEPOX-SOA). Other factors, in contrast, represented a wide range of sources that shared in-  
511 common processes (e.g., LO-OOA and MO-OOA). The clustering analysis contextualized the  
512 PMF results and demonstrated that the effects of the urban pollution were neither limited to nor  
513 captured by a single PMF factor. Instead, the urban plume influenced several PMF factors in  
514 different ways and to different extents. The implication is that changes in the AMS spectral  
515 signature of the organic PM caused by polluted conditions may not be sufficiently unique to  
516 allow for its complete separation by PMF analysis alone, especially in respect to the production  
517 of secondary organic PM. In this context, the Fuzzy c-means analysis served herein as a useful  
518 tool to incorporate auxiliary datasets and thereby to further understand anthropogenic influences  
519 on PM production and characteristics.

#### 520 **4. Summary and conclusions**

521         Changes in the concentrations and the composition of fine-mode PM due to the influence  
522 of anthropogenic emissions were investigated for the Amazonian wet season. Organic material  
523 dominated the submicron composition, consistently representing between 70% and 80% of the  
524  $PM_{10}$  mean mass concentration across measurement sites upwind and downwind of Manaus and

525 across different levels of pollution. Absolute mass concentrations, however, varied significantly  
526 among sites. Average concentrations downwind of Manaus were 100% to 200% higher than  
527 those upwind. Furthest downwind at T3, the organic component was more oxidized compared to  
528 that at the T2 site.

529 Positive-matrix factorization and Fuzzy c-means clustering were applied to the datasets to  
530 obtain a composite analysis of the shifts in PM<sub>1</sub> concentrations and composition under polluted  
531 conditions. Based on the FCM clustering, every point in time at T3 was interpreted as being  
532 affected by a combination of four influences, as represented by four clusters. Two background  
533 (Bkgd-1 and Bkgd-2) and two polluted (Pol-1 and Pol-2) clusters were identified. Particle mass  
534 concentrations were double for polluted compared to background conditions. Contributions from  
535 secondary processes dominated (> 80%) for both background and polluted conditions.

536 In terms of primary emissions, absolute contributions increased by a factor of five or  
537 more under polluted conditions, corresponding to an increase from < 10% to 15% of total PM<sub>1</sub>.  
538 The ADOA factor loading increased over five-fold for the polluted compared to the background  
539 clusters, and this factor thus served as a strong tracer of Manaus pollution. BBOA and HOA  
540 factor loadings, associated with biomass burning and fossil fuels, respectively, increased by two-  
541 fold with pollution. The ADOA factor loading represented 61% to 76% of the total primary  
542 factor loadings for the Pol-1 and Pol-2 clusters.

543 As for the secondary processes, the analysis further finds that the pollution plume acted  
544 both to shift pathways of secondary organic PM production and to accelerate the atmospheric  
545 oxidation of pre-existing organic PM. The oxidation of biogenic PM precursors shifted from  
546 HO<sub>2</sub>- to NO-dominant pathways, and the oxidation of anthropogenic precursors possibly  
547 contributed to increased PM concentrations. The IEPOX-SOA factor loadings were highest for

548 the Bkgd-2 cluster, associated with long-range transport under background conditions, and  
549 decreased by almost 50% for the polluted clusters, in line with a shift of isoprene oxidation from  
550 HO<sub>2</sub>- to NO-dominant pathways. Concomitantly, the LO-OOA factor loading increased by more  
551 than 50% for these clusters, suggesting rapid in-plume production of secondary organic PM  
552 through several pathways. The LO-OOA factor was also important for the Bkgd-1 cluster,  
553 associated with fresh background conditions, which is suggestive of recent biogenic organic PM  
554 production. The MO-OOA factor had large relative contributions in the Bkgd-2, Pol-1, and Pol-2  
555 clusters, suggestive of significant oxidative processing associated with these clusters. Increases  
556 of up to 300% in the MO-OOA factor loadings for Pol-1 and Pol-2 relative to background  
557 conditions of Bkgd-1 showed the effects of an accelerated oxidation cycle, leading to highly  
558 oxidized PM downwind of Manaus. Based on this and related studies (Liu et al., 2016b; de Sá et  
559 al., 2017; Martin et al., 2017), the critical lever seems to be increased concentrations of nitrogen  
560 oxides in the pollution plume for both directly shifting and indirectly accelerating mechanisms of  
561 secondary organic PM production in central Amazonia during the wet season.

562         The altered composition under anthropogenic influences also affects the physical  
563 properties of the PM<sub>1</sub>. Bateman et al. (2017), using the results of the PMF analysis presented  
564 herein, reported a shift from predominantly liquid PM under background conditions to a  
565 considerable presence of non-liquid PM above 50% RH under polluted conditions. Non-liquid  
566 PM can have different reactive chemistry from liquid PM (Li et al., 2015; Liu et al., 2018). A  
567 linear relationship between the increase in particle rebound fraction and the sum of ADOA,  
568 BBOA, and HOA factor loadings had an  $R^2$  of 0.7. The highest individual correlation was with  
569 the ADOA factor loading (Bateman, personal communication). In addition, Thalman et al.  
570 (2017), also using the PMF results reported herein, concluded that the larger relative contribution

571 of secondary organic material during the daytime compared to the nighttime was the primary  
572 driver of the diel trend of higher particle hygroscopicity during the day compared to the night, as  
573 tied to cloud condensation nuclei (CCN) properties.

574 This study communicates a snapshot of the changes that occur in the atmospheric  
575 composition over a tropical forest because of regional urbanization. In the context of a forest in  
576 transition (Davidson et al., 2012), the findings herein provide a quantitative assessment of the  
577 effects of urban pollution on the forested surroundings of Manaus. The studied region and the  
578 observed changes in atmospheric composition represent a microcosm that might become more  
579 widespread through Amazonia as urbanization trends continue in the future. Further  
580 investigations of the specific chemical pathways and physical mechanisms that enhance PM  
581 production in the urban plume are warranted to understand what other pollutants are critical for  
582 control in the context of ongoing and future air quality regulation in the study region as well as  
583 for other tropical forested environments worldwide.

**Acknowledgments.** Institutional support was provided by the Central Office of the Large Scale Biosphere Atmosphere Experiment in Amazonia (LBA), the National Institute of Amazonian Research (INPA), and Amazonas State University (UEA). We acknowledge support from the Atmospheric Radiation Measurement (ARM) Climate Research Facility, a user facility of the United States Department of Energy (DOE, DE-SC0006680), Office of Science, sponsored by the Office of Biological and Environmental Research, and support from the Atmospheric System Research (ASR, DE-SC0011115, DE-SC0011105) program of that office. Additional funding was provided by the Amazonas State Research Foundation (FAPEAM 062.00568/2014 and 134/2016), the São Paulo State Research Foundation (FAPESP 2013/05014-0), the USA National Science Foundation (1106400 and 1332998), and the Brazilian Scientific Mobility Program (CsF/CAPES). S. S. de Sá acknowledges support by the Faculty for the Future Fellowship of the Schlumberger Foundation. BBP is grateful for a US EPA STAR Graduate Fellowship (FP-91761701-0). The authors thank Paulo Castillo for his assistance in quality-checking the black carbon data from MAOS. Data access from the Sistema de Proteção da Amazônia (SIPAM) is gratefully acknowledged. The research was conducted under scientific license 001030/2012-4 of the Brazilian National Council for Scientific and Technological Development (CNPq).

## References

- Andreae, M. O., Acevedo, O. C., Araùjo, A., Artaxo, P., Barbosa, C. G. G., Barbosa, H. M. J., Brito, J., Carbone, S., Chi, X., Cintra, B. B. L., da Silva, N. F., Dias, N. L., Dias-Júnior, C. Q., Ditas, F., Ditz, R., Godoi, A. F. L., Godoi, R. H. M., Heimann, M., Hoffmann, T., Kesselmeier, J., Könemann, T., Krüger, M. L., Lavric, J. V., Manzi, A. O., Lopes, A. P., Martins, D. L., Mikhailov, E. F., Moran-Zuloaga, D., Nelson, B. W., Nölscher, A. C., Santos Nogueira, D., Piedade, M. T. F., Pöhlker, C., Pöschl, U., Quesada, C. A., Rizzo, L. V., Ro, C. U., Ruckteschler, N., Sá, L. D. A., de Oliveira Sá, M., Sales, C. B., dos Santos, R. M. N., Saturno, J., Schöngart, J., Sörgel, M., de Souza, C. M., de Souza, R. A. F., Su, H., Targhetta, N., Tóta, J., Trebs, I., Trumbore, S., van Eijck, A., Walter, D., Wang, Z., Weber, B., Williams, J., Winderlich, J., Wittmann, F., Wolff, S., and Yáñez-Serrano, A. M.: The Amazon Tall Tower Observatory (ATTO): overview of pilot measurements on ecosystem ecology, meteorology, trace gases, and aerosols, *Atmos. Chem. Phys.*, 15, 18, 10723-10776, 2015, 10.5194/acp-15-10723-2015.
- Artaxo, P., Rizzo, L. V., Brito, J. F., Barbosa, H. M. J., Arana, A., Sena, E. T., Cirino, G. G., Bastos, W., Martin, S. T., and Andreae, M. O.: Atmospheric aerosols in Amazonia and land use change: from natural biogenic to biomass burning conditions, *Faraday Disc.*, 165, 0, 203-235, 2013, 10.1039/C3FD00052D.
- Bateman, A. P., Gong, Z., Harder, T. H., de Sá, S. S., Wang, B., Castillo, P., China, S., Liu, Y., O'Brien, R. E., Palm, B. B., Shiu, H. W., Cirino, G. G., Thalman, R., Adachi, K., Alexander, M. L., Artaxo, P., Bertram, A. K., Buseck, P. R., Gilles, M. K., Jimenez, J. L., Laskin, A., Manzi, A. O., Sedlacek, A., Souza, R. A. F., Wang, J., Zaveri, R., and Martin, S. T.: Anthropogenic influences on the physical state of submicron particulate matter over a tropical forest, *Atmos. Chem. Phys.*, 17, 3, 1759-1773, 2017, 10.5194/acp-17-1759-2017.
- Bezdek, J. C., Ehrlich, R., and Full, W.: FCM: The fuzzy c-means clustering algorithm, *Computers & Geosciences*, 10, 2, 191-203, 1984.
- Budisulistiorini, S. H., Canagaratna, M. R., Croteau, P. L., Marth, W. J., Baumann, K., Edgerton, E. S., Shaw, S. L., Knipping, E. M., Worsnop, D. R., Jayne, J. T., Gold, A., and Surratt, J. D.: Real-time continuous characterization of secondary organic aerosol derived from isoprene epoxydiols in downtown Atlanta, Georgia, using the Aerodyne Aerosol Chemical Speciation Monitor, *Environ. Sci. Technol.*, 47, 11, 5686-5694, 2013, 10.1021/es400023n.
- Budisulistiorini, S. H., Li, X., Bairai, S. T., Renfro, J., Liu, Y., Liu, Y. J., McKinney, K. A., Martin, S. T., McNeill, V. F., Pye, H. O. T., Nenes, A., Neff, M. E., Stone, E. A., Mueller, S., Knote, C., Shaw, S. L., Zhang, Z., Gold, A., and Surratt, J. D.: Examining the effects of anthropogenic emissions on isoprene-derived secondary organic aerosol formation during the 2013 Southern Oxidant and Aerosol Study (SOAS) at the Look Rock, Tennessee ground site, *Atmos. Chem. Phys.*, 15, 15, 8871-8888, 2015, 10.5194/acp-15-8871-2015.

- Canagaratna, M. R., Jayne, J. T., Jimenez, J. L., Allan, J. D., Alfarra, M. R., Zhang, Q., Onasch, T. B., Drewnick, F., Coe, H., Middlebrook, A., Delia, A., Williams, L. R., Trimborn, A. M., Northway, M. J., DeCarlo, P. F., Kolb, C. E., Davidovits, P., and Worsnop, D. R.: Chemical and microphysical characterization of ambient aerosols with the aerodyne aerosol mass spectrometer, *Mass Spectrom. Rev.*, 26, 2, 185-222, 2007, 10.1002/mas.20115.
- Canagaratna, M. R., Jimenez, J. L., Kroll, J. H., Chen, Q., Kessler, S. H., Massoli, P., Hildebrandt Ruiz, L., Fortner, E., Williams, L. R., Wilson, K. R., Surratt, J. D., Donahue, N. M., Jayne, J. T., and Worsnop, D. R.: Elemental ratio measurements of organic compounds using aerosol mass spectrometry: characterization, improved calibration, and implications, *Atmos. Chem. Phys.*, 15, 1, 253-272, 2015, 10.5194/acp-15-253-2015.
- Cappa, C. D., Lack, D. A., Burkholder, J. B., and Ravishankara, A. R.: Bias in filter-based aerosol light absorption measurements due to organic aerosol loading: evidence from laboratory Measurements, *Aerosol Sci Technol*, 42, 12, 1022-1032, 2008, 10.1080/02786820802389285.
- Carlton, A. G., Turpin, B. J., Lim, H.-J., Altieri, K. E., and Seitzinger, S.: Link between isoprene and secondary organic aerosol (SOA): Pyruvic acid oxidation yields low volatility organic acids in clouds, *Geophys. Res. Lett.*, 33, 6, L06822, 2006, 10.1029/2005GL025374.
- Carlton, A. G., Pinder, R. W., Bhawe, P. V., and Pouliot, G. A.: To What Extent Can Biogenic SOA be Controlled?, *Environ. Sci. Technol.*, 44, 9, 3376-3380, 2010, 10.1021/es903506b.
- Chen, Q., Farmer, D. K., Schneider, J., Zorn, S. R., Heald, C. L., Karl, T. G., Guenther, A., Allan, J. D., Robinson, N., Coe, H., Kimmel, J. R., Pauliquevis, T., Borrmann, S., Pöschl, U., Andreae, M. O., Artaxo, P., Jimenez, J. L., and Martin, S. T.: Mass spectral characterization of submicron biogenic organic particles in the Amazon Basin, *Geophys. Res. Lett.*, 36, 20, L20806, 2009, 10.1029/2009GL039880.
- Chen, Q., Farmer, D. K., Rizzo, L. V., Pauliquevis, T., Kuwata, M., Karl, T. G., Guenther, A., Allan, J. D., Coe, H., Andreae, M. O., Pöschl, U., Jimenez, J. L., Artaxo, P., and Martin, S. T.: Submicron particle mass concentrations and sources in the Amazonian wet season (AMAZE-08), *Atmos. Chem. Phys.*, 15, 7, 3687-3701, 2015, 10.5194/acp-15-3687-2015.
- Chhabra, P., Ng, N., Canagaratna, M., Corrigan, A., Russell, L., Worsnop, D., Flagan, R., and Seinfeld, J.: Elemental composition and oxidation of chamber organic aerosol, *Atmos. Chem. Phys.*, 11, 17, 8827-8845, 2011.
- Cirino, G. G., Brito, J., Barbosa, H. J. M., Rizzo, L. V., Tunved, P., de Sá, S. S., Jimenez, J., Palm, B. B., Carbone, S., Lavric, J., Souza, R., Wolff, S., Walter, D., Tota, J., Oliveira, M., Martin, S. T., and Artaxo, P.: Observations of Manaus urban plume evolution and interaction with biogenic emissions in GoAmazon2014/5, *Atmos Environ*, submitted.
- Cubison, M. J., Ortega, A. M., Hayes, P. L., Farmer, D. K., Day, D., Lechner, M. J., Brune, W. H., Apel, E., Diskin, G. S., Fisher, J. A., Fuelberg, H. E., Hecobian, A., Knapp, D. J., Mikoviny, T., Riemer, D., Sachse, G. W., Sessions, W., Weber, R. J., Weinheimer, A. J., Wisthaler, A., and Jimenez, J. L.: Effects of aging on organic aerosol from open biomass burning smoke in aircraft and laboratory studies, *Atmos. Chem. Phys.*, 11, 23, 12049-12064, 2011, 10.5194/acp-11-12049-2011.



- Davidson, E. A., de Araújo, A. C., Artaxo, P., Balch, J. K., Brown, I. F., Bustamante, M. M., Coe, M. T., DeFries, R. S., Keller, M., and Longo, M.: The Amazon basin in transition, *Nature*, 481, 7381, 321-328, 2012.
- De Gouw, J. and Jimenez, J. L.: Organic Aerosols in the Earth's Atmosphere, *Environ. Sci. Technol.*, 43, 20, 7614-7618, 2009, 10.1021/es9006004.
- de Gouw, J. A., Middlebrook, A. M., Warneke, C., Goldan, P. D., Kuster, W. C., Roberts, J. M., Fehsenfeld, F. C., Worsnop, D. R., Canagaratna, M. R., Pszenny, A. A. P., Keene, W. C., Marchewka, M., Bertman, S. B., and Bates, T. S.: Budget of organic carbon in a polluted atmosphere: Results from the New England Air Quality Study in 2002, *J. Geophys. Res. Atmos.*, 110, D16, D16305, 2005, 10.1029/2004JD005623.
- de Gouw, J. A., Brock, C. A., Atlas, E. L., Bates, T. S., Fehsenfeld, F. C., Goldan, P. D., Holloway, J. S., Kuster, W. C., Lerner, B. M., Matthew, B. M., Middlebrook, A. M., Onasch, T. B., Peltier, R. E., Quinn, P. K., Senff, C. J., Stohl, A., Sullivan, A. P., Trainer, M., Warneke, C., Weber, R. J., and Williams, E. J.: Sources of particulate matter in the northeastern United States in summer: 1. Direct emissions and secondary formation of organic matter in urban plumes, *J. Geophys. Res. Atmos.*, 113, D8, D08301, 2008, 10.1029/2007JD009243.
- de Sá, S. S., Palm, B. B., Campuzano-Jost, P., Day, D. A., Newburn, M. K., Hu, W., Isaacman-VanWertz, G., Yee, L. D., Thalman, R., Brito, J., Carbone, S., Artaxo, P., Goldstein, A. H., Manzi, A. O., Souza, R. A. F., Mei, F., Shilling, J. E., Springston, S. R., Wang, J., Surratt, J. D., Alexander, M. L., Jimenez, J. L., and Martin, S. T.: Influence of urban pollution on the production of organic particulate matter from isoprene epoxydiols in central Amazonia, *Atmos. Chem. Phys.*, 17, 11, 6611-6629, 2017, 10.5194/acp-17-6611-2017.
- DeCarlo, P. F., Kimmel, J. R., Trimborn, A., Northway, M. J., Jayne, J. T., Aiken, A. C., Gonin, M., Fuhrer, K., Horvath, T., Docherty, K. S., Worsnop, D. R., and Jimenez, J. L.: Field-deployable, high-resolution, time-of-flight aerosol mass spectrometer, *Anal. Chem.*, 78, 24, 8281-8289, 2006, 10.1021/ac061249n.
- dos Santos, M. J., Silva Dias, M. A. F., and Freitas, E. D.: Influence of local circulations on wind, moisture, and precipitation close to Manaus City, Amazon Region, Brazil, *J. Geophys. Res. Atmos.*, 119, 23, 13,233-213,249, 2014, 10.1002/2014JD021969.
- Draxler, R. and Hess, G.: An overview of the HYSPLIT\_4 modeling system for trajectories, dispersion, and deposition, *Aust. Met. Mag.*, 47, 295-308, 1998.
- Ervens, B., Turpin, B., and Weber, R.: Secondary organic aerosol formation in cloud droplets and aqueous particles (aqSOA): a review of laboratory, field and model studies, *Atmos. Chem. Phys.*, 11, 21, 11069-11102, 2011, 10.5194/acp-11-11069-2011.
- Farmer, D. K., Matsunaga, A., Docherty, K. S., Surratt, J. D., Seinfeld, J. H., Ziemann, P. J., and Jimenez, J. L.: Response of an aerosol mass spectrometer to organonitrates and organosulfates and implications for atmospheric chemistry, *Proc. Natl. Acad. Sci. USA*, 107, 15, 6670-6675, 2010, 10.1073/pnas.0912340107.
- Fry, J. L., Kiendler-Scharr, A., Rollins, A. W., Wooldridge, P. J., Brown, S. S., Fuchs, H., Dubé, W., Mensah, A., dal Maso, M., Tillmann, R., Dorn, H. P., Brauers, T., and Cohen, R. C.: Organic nitrate and secondary organic aerosol yield from NO<sub>3</sub> oxidation of  $\beta$ -pinene evaluated using a gas-phase kinetics/aerosol partitioning model, *Atmos. Chem. Phys.*, 9, 4, 1431-1449, 2009, 10.5194/acp-9-1431-2009.

- Fry, J. L., Draper, D. C., Zarzana, K. J., Campuzano-Jost, P., Day, D. A., Jimenez, J. L., Brown, S. S., Cohen, R. C., Kaser, L., Hansel, A., Cappellin, L., Karl, T., Hodzic Roux, A., Turnipseed, A., Cantrell, C., Lefer, B. L., and Grossberg, N.: Observations of gas- and aerosol-phase organic nitrates at BEACHON-RoMBAS 2011, *Atmos. Chem. Phys.*, 13, 17, 8585-8605, 2013, 10.5194/acp-13-8585-2013.
- Glasius, M. and Goldstein, A. H.: Recent discoveries and future challenges in atmospheric organic chemistry, *Environ. Sci. Technol.*, 50, 6, 2754-2764, 2016, 10.1021/acs.est.5b05105.
- Goldstein, A. H., Koven, C. D., Heald, C. L., and Fung, I. Y.: Biogenic carbon and anthropogenic pollutants combine to form a cooling haze over the southeastern United States, *Proc. Natl Acad. Sci. USA*, 106, 22, 8835-8840, 2009, 10.1073/pnas.0904128106.
- Guenther, A., Jiang, X., Heald, C., Sakulyanontvittaya, T., Duhl, T., Emmons, L., and Wang, X.: The Model of Emissions of Gases and Aerosols from Nature version 2.1 (MEGAN2. 1): an extended and updated framework for modeling biogenic emissions, *Geosci. Model Dev.*, 5, 6, 1471-1492, 2012, 10.5194/gmd-5-1471-2012.
- Hallquist, M., Wenger, J. C., Baltensperger, U., Rudich, Y., Simpson, D., Claeys, M., Dommen, J., Donahue, N. M., George, C., Goldstein, A. H., Hamilton, J. F., Herrmann, H., Hoffmann, T., Iinuma, Y., Jang, M., Jenkin, M. E., Jimenez, J. L., Kiendler-Scharr, A., Maenhaut, W., McFiggans, G., Mentel, T. F., Monod, A., Prévôt, A. S. H., Seinfeld, J. H., Surratt, J. D., Szmigielski, R., and Wildt, J.: The formation, properties and impact of secondary organic aerosol: current and emerging issues, *Atmos. Chem. Phys.*, 9, 14, 5155-5236, 2009, 10.5194/acp-9-5155-2009.
- Heald, C. L., Coe, H., Jimenez, J. L., Weber, R. J., Bahreini, R., Middlebrook, A. M., Russell, L. M., Jolleys, M., Fu, T. M., Allan, J. D., Bower, K. N., Capes, G., Crosier, J., Morgan, W. T., Robinson, N. H., Williams, P. I., Cubison, M. J., DeCarlo, P. F., and Dunlea, E. J.: Exploring the vertical profile of atmospheric organic aerosol: comparing 17 aircraft field campaigns with a global model, *Atmos. Chem. Phys.*, 11, 24, 12673-12696, 2011, 10.5194/acp-11-12673-2011.
- Hou, A. Y., Kakar, R. K., Neeck, S., Azarbarzin, A. A., Kummerow, C. D., Kojima, M., Oki, R., Nakamura, K., and Iguchi, T.: The Global Precipitation Measurement mission, *Bull. Am. Meteorol. Soc.*, 95, 5, 701-722, 2014, 10.1175/bams-d-13-00164.1.
- Hoyle, C. R., Myhre, G., Berntsen, T. K., and Isaksen, I. S. A.: Anthropogenic influence on SOA and the resulting radiative forcing, *Atmos. Chem. Phys.*, 9, 8, 2715-2728, 2009, 10.5194/acp-9-2715-2009.
- Hoyle, C. R., Boy, M., Donahue, N. M., Fry, J. L., Glasius, M., Guenther, A., Hallar, A. G., Huff Hartz, K., Petters, M. D., Petäjä, T., Rosenoern, T., and Sullivan, A. P.: A review of the anthropogenic influence on biogenic secondary organic aerosol, *Atmos. Chem. Phys.*, 11, 1, 321-343, 2011, 10.5194/acp-11-321-2011.
- Hu, W., Hu, M., Hu, W., Jimenez, J. L., Yuan, B., Chen, W., Wang, M., Wu, Y., Chen, C., Wang, Z., Peng, J., Zeng, L., and Shao, M.: Chemical composition, sources, and aging process of submicron aerosols in Beijing: Contrast between summer and winter, *J. Geophys. Res. Atmos.*, 121, 4, 1955-1977, 2016, 10.1002/2015JD024020.
- Hu, W. W., Campuzano-Jost, P., Palm, B. B., Day, D. A., Ortega, A. M., Hayes, P. L., Krechmer, J. E., Chen, Q., Kuwata, M., Liu, Y. J., de Sá, S. S., McKinney, K., Martin, S. T., Hu, M., Budisulistiorini, S. H., Riva, M., Surratt, J. D., St. Clair, J. M., Isaacman-Van Wertz, G., Yee, L. D., Goldstein, A. H., Carbone, S., Brito, J., Artaxo, P., de Gouw, J. A.,

- Koss, A., Wisthaler, A., Mikoviny, T., Karl, T., Kaser, L., Jud, W., Hansel, A., Docherty, K. S., Alexander, M. L., Robinson, N. H., Coe, H., Allan, J. D., Canagaratna, M. R., Paulot, F., and Jimenez, J. L.: Characterization of a real-time tracer for isoprene epoxydiols-derived secondary organic aerosol (IEPOX-SOA) from aerosol mass spectrometer measurements, *Atmos. Chem. Phys.*, 15, 20, 11807-11833, 2015, 10.5194/acp-15-11807-2015.
- Huang, R.-J., Zhang, Y., Bozzetti, C., Ho, K.-F., Cao, J.-J., Han, Y., Daellenbach, K. R., Slowik, J. G., Platt, S. M., Canonaco, F., Zotter, P., Wolf, R., Pieber, S. M., Bruns, E. A., Crippa, M., Ciarelli, G., Piazzalunga, A., Schwikowski, M., Abbaszade, G., Schnelle-Kreis, J., Zimmermann, R., An, Z., Szidat, S., Baltensperger, U., Haddad, I. E., and Prevot, A. S. H.: High secondary aerosol contribution to particulate pollution during haze events in China, *Nature*, 514, 7521, 218-222, 2014, 10.1038/nature13774.
- Isaacman-VanWertz, G., Yee, L. D., Kreisberg, N. M., Wernis, R., Moss, J. A., Hering, S. V., de Sá, S. S., Martin, S. T., Alexander, M. L., Palm, B. B., Hu, W., Campuzano-Jost, P., Day, D. A., Jimenez, J. L., Riva, M., Surratt, J. D., Viegas, J., Manzi, A., Edgerton, E., Baumann, K., Souza, R., Artaxo, P., and Goldstein, A. H.: Ambient Gas-Particle Partitioning of Tracers for Biogenic Oxidation, *Environ. Sci. Technol.*, 9952-9962, 2016, 10.1021/acs.est.6b01674.
- Jimenez, J. L., Canagaratna, M. R., Donahue, N. M., Prevot, A. S. H., Zhang, Q., Kroll, J. H., DeCarlo, P. F., Allan, J. D., Coe, H., Ng, N. L., Aiken, A. C., Docherty, K. S., Ulbrich, I. M., Grieshop, A. P., Robinson, A. L., Duplissy, J., Smith, J. D., Wilson, K. R., Lanz, V. A., Hueglin, C., Sun, Y. L., Tian, J., Laaksonen, A., Raatikainen, T., Rautiainen, J., Vaattovaara, P., Ehn, M., Kulmala, M., Tomlinson, J. M., Collins, D. R., Cubison, M. J., Dunlea, J., Huffman, J. A., Onasch, T. B., Alfarra, M. R., Williams, P. I., Bower, K., Kondo, Y., Schneider, J., Drewnick, F., Borrmann, S., Weimer, S., Demerjian, K., Salcedo, D., Cottrell, L., Griffin, R., Takami, A., Miyoshi, T., Hatakeyama, S., Shimojo, A., Sun, J. Y., Zhang, Y. M., Dzepina, K., Kimmel, J. R., Sueper, D., Jayne, J. T., Herndon, S. C., Trimborn, A. M., Williams, L. R., Wood, E. C., Middlebrook, A. M., Kolb, C. E., Baltensperger, U., and Worsnop, D. R.: Evolution of organic aerosols in the atmosphere, *Science*, 326, 5959, 1525-1529, 2009, 10.1126/science.1180353.
- Joss, J. and Waldvogel, A.: Ein Spektrograph für Niederschlagstropfen mit automatischer Auswertung, *Pure and Applied Geophysics*, 68, 1, 240-246, 1967, 10.1007/BF00874898.
- Krechmer, J. E., Coggon, M. M., Massoli, P., Nguyen, T. B., Crouse, J. D., Hu, W., Day, D. A., Tyndall, G. S., Henze, D. K., Rivera-Rios, J. C., Nowak, J. B., Kimmel, J. R., Mauldin, R. L., Stark, H., Jayne, J. T., Sipilä, M., Junninen, H., Clair, J. M. S., Zhang, X., Feiner, P. A., Zhang, L., Miller, D. O., Brune, W. H., Keutsch, F. N., Wennberg, P. O., Seinfeld, J. H., Worsnop, D. R., Jimenez, J. L., and Canagaratna, M. R.: Formation of low volatility organic compounds and secondary organic aerosol from isoprene hydroxyhydroperoxide low-NO oxidation, *Environ. Sci. Technol.*, 49, 17, 10330-10339, 2015, 10.1021/acs.est.5b02031.
- Kroll, J. H., Ng, N. L., Murphy, S. M., Flagan, R. C., and Seinfeld, J. H.: Secondary organic aerosol formation from isoprene photooxidation under high-NO<sub>x</sub> conditions, *Geophys. Res. Lett.*, 32, 18, 2005, 10.1029/2005GL023637.
- Kroll, J. H., Ng, N. L., Murphy, S. M., Flagan, R. C., and Seinfeld, J. H.: Secondary organic aerosol formation from isoprene photooxidation, *Environ. Sci. Technol.*, 40, 6, 1869-1877, 2006, 10.1021/es0524301.

- Kuhn, U., Ganzeveld, L., Thielmann, A., Dindorf, T., Schebeske, G., Welling, M., Sciare, J., Roberts, G., Meixner, F. X., Kesselmeier, J., Lelieveld, J., Kolle, O., Ciccioli, P., Lloyd, J., Trentmann, J., Artaxo, P., and Andreae, M. O.: Impact of Manaus City on the Amazon Green Ocean atmosphere: ozone production, precursor sensitivity and aerosol load, *Atmos. Chem. Phys.*, 10, 19, 9251-9282, 2010, 10.5194/acp-10-9251-2010.
- Kummerow, C., Barnes, W., Kozu, T., Shiue, J., and Simpson, J.: The Tropical Rainfall Measuring Mission (TRMM) sensor package, *J. Atmos. Ocea. Technol.*, 15, 3, 809-817, 1998, 10.1175/1520-0426(1998)015<0809:ttrmmt>2.0.co;2.
- Kuwata, M., Liu, Y., McKinney, K., and Martin, S. T.: Physical state and acidity of inorganic sulfate can regulate the production of secondary organic material from isoprene photooxidation products, *Phys. Chem. Chem. Phys.*, 17, 8, 5670-5678, 2015, 10.1039/C4CP04942J.
- Lack, D. A., Cappa, C. D., Covert, D. S., Baynard, T., Massoli, P., Sierau, B., Bates, T. S., Quinn, P. K., Lovejoy, E. R., and Ravishankara, A. R.: Bias in filter-based aerosol light absorption measurements due to organic aerosol loading: evidence from ambient measurements, *Aerosol Sci Technol*, 42, 12, 1033-1041, 2008, 10.1080/02786820802389277.
- Lambe, A. T., Onasch, T. B., Massoli, P., Croasdale, D. R., Wright, J. P., Ahern, A. T., Williams, L. R., Worsnop, D. R., Brune, W. H., and Davidovits, P.: Laboratory studies of the chemical composition and cloud condensation nuclei (CCN) activity of secondary organic aerosol (SOA) and oxidized primary organic aerosol (OPOA), *Atmos. Chem. Phys.*, 11, 17, 8913-8928, 2011, 10.5194/acp-11-8913-2011.
- Lanz, V. A., Alfarra, M. R., Baltensperger, U., Buchmann, B., Hueglin, C., and Prévôt, A. S. H.: Source apportionment of submicron organic aerosols at an urban site by factor analytical modelling of aerosol mass spectra, *Atmos. Chem. Phys.*, 7, 6, 1503-1522, 2007, 10.5194/acp-7-1503-2007.
- Li, Y. J., Liu, P., Gong, Z., Wang, Y., Bateman, A. P., Bergoend, C., Bertram, A. K., and Martin, S. T.: Chemical reactivity and liquid/nonliquid states of secondary organic material, *Environ. Sci. Technol.*, 49, 22, 13264-13274, 2015, 10.1021/acs.est.5b03392.
- Liao, J., Froyd, K. D., Murphy, D. M., Keutsch, F. N., Yu, G., Wennberg, P. O., St. Clair, J. M., Crounse, J. D., Wisthaler, A., Mikoviny, T., Jimenez, J. L., Campuzano-Jost, P., Day, D. A., Hu, W., Ryerson, T. B., Pollack, I. B., Peischl, J., Anderson, B. E., Ziemba, L. D., Blake, D. R., Meinardi, S., and Diskin, G.: Airborne measurements of organosulfates over the continental US, *J. Geophys. Res. Atmos.*, 120, 7, 2990-3005, 2015, 10.1002/2014JD022378.
- Lin, Y.-H., Zhang, Z., Docherty, K. S., Zhang, H., Budisulistiorini, S. H., Rubitschun, C. L., Shaw, S. L., Knipping, E. M., Edgerton, E. S., Kleindienst, T. E., Gold, A., and Surratt, J. D.: Isoprene epoxydiols as precursors to secondary organic aerosol formation: acid-catalyzed reactive uptake studies with authentic compounds, *Environ. Sci. Technol.*, 46, 1, 250-258, 2012, 10.1021/es202554c.
- Liu, J., D'Ambro, E. L., Lee, B. H., Lopez-Hilfiker, F. D., Zaveri, R. A., Rivera-Rios, J. C., Keutsch, F. N., Iyer, S., Kurten, T., Zhang, Z., Gold, A., Surratt, J. D., Shilling, J. E., and Thornton, J. A.: Efficient isoprene secondary organic aerosol formation from a non-IEPOX pathway, *Environ. Sci. Technol.*, 2016a, 10.1021/acs.est.6b01872.

- Liu, P., Li, Y. J., Wang, Y., Bateman, A. P., Zhang, Y., Gong, Z., Bertram, A. K., and Martin, S. T.: Highly viscous states affect the browning of atmospheric organic particulate matter, *ACS Cent Sci*, 2018, 10.1021/acscentsci.7b00452.
- Liu, Y., Brito, J., Dorris, M. R., Rivera-Rios, J. C., Seco, R., Bates, K. H., Artaxo, P., Duvoisin, S., Keutsch, F. N., Kim, S., Goldstein, A. H., Guenther, A. B., Manzi, A. O., Souza, R. A. F., Springston, S. R., Watson, T. B., McKinney, K. A., and Martin, S. T.: Isoprene photochemistry over the Amazon rain forest, *Proc. Natl. Acad. Sci. USA*, 113, 22, 6125-6130, 2016b, 10.1073/pnas.1524136113.
- Liu, Y., Seco, R., Kim, S., Guenther, A. B., Goldstein, A. H., Keutsch, F. N., Springston, S. R., Watson, T. B., Artaxo, P., Souza, R. A. F., McKinney, K. A., and Martin, S. T.: Isoprene photo-oxidation products quantify the effect of pollution on hydroxyl radicals over Amazonia, *Science Advances*, accepted.
- Machado, L. A. T., Dias, M. A. F. S., Morales, C., Fisch, G., Vila, D., Albrecht, R., Goodman, S. J., Calheiros, A. J. P., Biscaro, T., Kummerow, C., Cohen, J., Fitzjarrald, D., Nascimento, E. L., Sakamoto, M. S., Cunningham, C., Chaboureaud, J.-P., Petersen, W. A., Adams, D. K., Baldini, L., Angelis, C. F., Sapucci, L. F., Salio, P., Barbosa, H. M. J., Landulfo, E., Souza, R. A. F., Blakeslee, R. J., Bailey, J., Freitas, S., Lima, W. F. A., and Tokay, A.: The Chuva Project: how does convection vary across Brazil?, *Bull. Am. Meteorol. Soc.*, 95, 9, 1365-1380, 2014, 10.1175/bams-d-13-00084.1.
- Martin, S. T., Andreae, M. O., Artaxo, P., Baumgardner, D., Chen, Q., Goldstein, A. H., Guenther, A., Heald, C. L., Mayol-Bracero, O. L., McMurry, P. H., Pauliquevis, T., Pöschl, U., Prather, K. A., Roberts, G. C., Saleska, S. R., Silva Dias, M. A., Spracklen, D. V., Swietlicki, E., and Trebs, I.: Sources and properties of Amazonian aerosol particles, *Rev. Geophys.*, 48, 2, RG2012, 2010a, 10.1029/2008RG000280.
- Martin, S. T., Andreae, M. O., Althausen, D., Artaxo, P., Baars, H., Borrmann, S., Chen, Q., Farmer, D. K., Guenther, A., Gunthe, S. S., Jimenez, J. L., Karl, T., Longo, K., Manzi, A., Müller, T., Pauliquevis, T., Petters, M. D., Prenni, A. J., Pöschl, U., Rizzo, L. V., Schneider, J., Smith, J. N., Swietlicki, E., Tota, J., Wang, J., Wiedensohler, A., and Zorn, S. R.: An overview of the Amazonian aerosol characterization experiment 2008 (AMAZE-08), *Atmos. Chem. Phys.*, 10, 23, 11415-11438, 2010b, 10.5194/acp-10-11415-2010.
- Martin, S. T., Artaxo, P., Machado, L. A. T., Manzi, A. O., Souza, R. A. F., Schumacher, C., Wang, J., Andreae, M. O., Barbosa, H. M. J., Fan, J., Fisch, G., Goldstein, A. H., Guenther, A., Jimenez, J. L., Pöschl, U., Silva Dias, M. A., Smith, J. N., and Wendisch, M.: Introduction: observations and modeling of the green ocean Amazon (GoAmazon2014/5), *Atmos. Chem. Phys.*, 16, 8, 4785-4797, 2016, 10.5194/acp-16-4785-2016.
- Martin, S. T., Artaxo, P., Machado, L., Manzi, A. O., Souza, R. A. F., Schumacher, C., Wang, J., Biscaro, T., Brito, J., Calheiros, A., Jardine, K., Medeiros, A., Portela, B., Sá, S. S. d., Adachi, K., Aiken, A. C., Albrecht, R., Alexander, L., Andreae, M. O., Barbosa, H. M. J., Buseck, P., Chand, D., Comstock, J. M., Day, D. A., Dubey, M., Fan, J., Fast, J., Fisch, G., Fortner, E., Giangrande, S., Gilles, M., Goldstein, A. H., Guenther, A., Hubbe, J., Jensen, M., Jimenez, J. L., Keutsch, F. N., Kim, S., Kuang, C., Laskin, A., McKinney, K., Mei, F., Miller, M., Nascimento, R., Pauliquevis, T., Pekour, M., Peres, J., Petäjä, T., Pöhlker, C., Pöschl, U., Rizzo, L., Schmid, B., Shilling, J. E., Dias, M. A. S., Smith, J. N., Tomlinson, J. M., Tóta, J., and Wendisch, M.: The Green Ocean Amazon Experiment

- (GoAmazon2014/5) observes pollution affecting gases, aerosols, clouds, and rainfall over the rain forest, *Bulletin of the American Meteorological Society*, 98, 5, 981-997, 2017, 10.1175/bams-d-15-00221.1.
- Medeiros, A. S. S., Calderaro, G., Guimarães, P. C., Magalhaes, M. R., Morais, M. V. B., Rafee, S. A. A., Ribeiro, I. O., Andreoli, R. V., Martins, J. A., Martins, L. D., Martin, S. T., and Souza, R. A. F.: Power plant fuel switching and air quality in a tropical, forested environment, *Atmos. Chem. Phys.*, 17, 14, 8987-8998, 2017, 10.5194/acp-17-8987-2017.
- Mohr, C., DeCarlo, P. F., Heringa, M. F., Chirico, R., Slowik, J. G., Richter, R., Reche, C., Alastuey, A., Querol, X., Seco, R., Peñuelas, J., Jiménez, J. L., Crippa, M., Zimmermann, R., Baltensperger, U., and Prévôt, A. S. H.: Identification and quantification of organic aerosol from cooking and other sources in Barcelona using aerosol mass spectrometer data, *Atmos. Chem. Phys.*, 12, 4, 1649-1665, 2012, 10.5194/acp-12-1649-2012.
- Ng, N., Canagaratna, M., Jimenez, J., Chhabra, P., Seinfeld, J., and Worsnop, D.: Changes in organic aerosol composition with aging inferred from aerosol mass spectra, *Atmos. Chem. Phys.*, 11, 13, 6465-6474, 2011a, 10.5194/acp-11-6465-2011.
- Ng, N. L., Canagaratna, M. R., Jimenez, J. L., Zhang, Q., Ulbrich, I. M., and Worsnop, D. R.: Real-time methods for estimating organic component mass concentrations from aerosol mass spectrometer data, *Environ. Sci. Technol.*, 45, 3, 910-916, 2011b, 10.1021/es102951k.
- Nguyen, T. B., Coggon, M. M., Bates, K. H., Zhang, X., Schwantes, R. H., Schilling, K. A., Loza, C. L., Flagan, R. C., Wennberg, P. O., and Seinfeld, J. H.: Organic aerosol formation from the reactive uptake of isoprene epoxydiols (IEPOX) onto non-acidified inorganic seeds, *Atmos. Chem. Phys.*, 14, 7, 3497-3510, 2014, 10.5194/acp-14-3497-2014.
- Nordin, E. Z., Eriksson, A. C., Roldin, P., Nilsson, P. T., Carlsson, J. E., Kajos, M. K., Hellén, H., Wittbom, C., Rissler, J., Löndahl, J., Swietlicki, E., Svenningsson, B., Bohgard, M., Kulmala, M., Hallquist, M., and Pagels, J. H.: Secondary organic aerosol formation from idling gasoline passenger vehicle emissions investigated in a smog chamber, *Atmos. Chem. Phys.*, 13, 12, 6101-6116, 2013, 10.5194/acp-13-6101-2013.
- Odum, J. R., Hoffmann, T., Bowman, F., Collins, D., Flagan, R. C., and Seinfeld, J. H.: Gas/particle partitioning and secondary organic aerosol yields, *Environ. Sci. Technol.*, 30, 8, 2580-2585, 1996, 10.1021/es950943+.
- Palm, B. B., de Sá, S. S., Day, D. A., Campuzano-Jost, P., Hu, W., Seco, R., Sjostedt, S. J., Park, J. H., Guenther, A. B., Kim, S., Brito, J., Wurm, F., Artaxo, P., Thalman, R., Wang, J., Yee, L. D., Wernis, R., Isaacman-VanWertz, G., Goldstein, A. H., Liu, Y., Springston, S. R., Souza, R., Newburn, M. K., Alexander, M. L., Martin, S. T., and Jimenez, J. L.: Secondary organic aerosol formation from ambient air in an oxidation flow reactor in central Amazonia, *Atmos. Chem. Phys.*, 18, 1, 467-493, 2018, 10.5194/acp-18-467-2018.
- Pankow, J. F.: An absorption model of gas/particle partitioning of organic compounds in the atmosphere, *Atmos. Environ.*, 28, 2, 185-188, 1994, 10.1016/1352-2310(94)90093-0.
- Paulot, F., Crounse, J. D., Kjaergaard, H. G., Kürten, A., Clair, J. M. S., Seinfeld, J. H., and Wennberg, P. O.: Unexpected epoxide formation in the gas-phase photooxidation of isoprene, *Science*, 325, 5941, 730-733, 2009, 10.1126/science.1172910.
- Perraud, V., Bruns, E. A., Ezell, M. J., Johnson, S. N., Yu, Y., Alexander, M. L., Zelenyuk, A., Imre, D., Chang, W. L., Dabdub, D., Pankow, J. F., and Finlayson-Pitts, B. J.:

- Nonequilibrium atmospheric secondary organic aerosol formation and growth, *Proc. Natl Acad. Sci. USA*, 109, 8, 2836-2841, 2012, 10.1073/pnas.1119909109.
- Pöhlker, M. L., Ditas, F., Saturno, J., Klimach, T., Hrabě de Angelis, I., Araújo, A., Brito, J., Carbone, S., Cheng, Y., Chi, X., Ditz, R., Gunthe, S. S., Kandler, K., Kesselmeier, J., Könemann, T., Lavrič, J. V., Martin, S. T., Mikhailov, E., Moran-Zuloaga, D., Rizzo, L. V., Rose, D., Su, H., Thalman, R., Walter, D., Wang, J., Wolff, S., Barbosa, H. M. J., Artaxo, P., Andreae, M. O., Pöschl, U., and Pöhlker, C.: Long-term observations of cloud condensation nuclei in the Amazon rain forest – Part 2: Variability and characteristic differences under near-pristine, biomass burning, and long-range transport conditions, *Atmos. Chem. Phys. Discuss.*, 2017, 1-51, 2017, 10.5194/acp-2017-847.
- Presto, A. A., Gordon, T. D., and Robinson, A. L.: Primary to secondary organic aerosol: evolution of organic emissions from mobile combustion sources, *Atmos. Chem. Phys.*, 14, 10, 5015-5036, 2014, 10.5194/acp-14-5015-2014.
- Riva, M., Budisulistiorini, S. H., Chen, Y., Zhang, Z., D'Ambro, E. L., Zhang, X., Gold, A., Turpin, B. J., Thornton, J. A., Canagaratna, M. R., and Surratt, J. D.: Chemical characterization of secondary organic aerosol from oxidation of isoprene hydroxyhydroperoxides, *Environ. Sci. Technol.*, 2016, 10.1021/acs.est.6b02511.
- Robinson, A. L., Donahue, N. M., Shrivastava, M. K., Weitkamp, E. A., Sage, A. M., Grieshop, A. P., Lane, T. E., Pierce, J. R., and Pandis, S. N.: Rethinking organic aerosols: semivolatile emissions and photochemical aging, *Science*, 315, 5816, 1259-1262, 2007, 10.1126/science.1133061.
- Robinson, N. H., Hamilton, J. F., Allan, J. D., Langford, B., Oram, D. E., Chen, Q., Docherty, K., Farmer, D. K., Jimenez, J. L., Ward, M. W., Hewitt, C. N., Barley, M. H., Jenkin, M. E., Rickard, A. R., Martin, S. T., McFiggans, G., and Coe, H.: Evidence for a significant proportion of Secondary Organic Aerosol from isoprene above a maritime tropical forest, *Atmos. Chem. Phys.*, 11, 3, 1039-1050, 2011, 10.5194/acp-11-1039-2011.
- Röhl, A. and Lammel, G.: Determination of malic acid and other C4 dicarboxylic acids in atmospheric aerosol samples, *Chemosphere*, 46, 8, 1195-1199, 2002, doi.org/10.1016/S0045-6535(01)00243-0.
- Schneider, J., Weimer, S., Drewnick, F., Borrmann, S., Helas, G., Gwaze, P., Schmid, O., Andreae, M. O., and Kirchner, U.: Mass spectrometric analysis and aerodynamic properties of various types of combustion-related aerosol particles, *Int. J. Mass Spectrom.*, 258, 1, 37-49, 2006, 10.1016/j.ijms.2006.07.008.
- Schneider, J., Freutel, F., Zorn, S., Chen, Q., Farmer, D., Jimenez, J., Martin, S., Artaxo, P., Wiedensohler, A., and Borrmann, S.: Mass-spectrometric identification of primary biological particle markers and application to pristine submicron aerosol measurements in Amazonia, *Atmos Chem Phys*, 11, 22, 11415-11429, 2011, doi.org/10.5194/acp-11-11415-2011.
- Setyan, A., Zhang, Q., Merkel, M., Knighton, W. B., Sun, Y., Song, C., Shilling, J. E., Onasch, T. B., Herndon, S. C., Worsnop, D. R., Fast, J. D., Zaveri, R. A., Berg, L. K., Wiedensohler, A., Flowers, B. A., Dubey, M. K., and Subramanian, R.: Characterization of submicron particles influenced by mixed biogenic and anthropogenic emissions using high-resolution aerosol mass spectrometry: results from CARES, *Atmos. Chem. Phys.*, 12, 17, 8131-8156, 2012, 10.5194/acp-12-8131-2012.
- Shilling, J. E., Zaveri, R. A., Fast, J. D., Kleinman, L., Alexander, M. L., Canagaratna, M. R., Fortner, E., Hubbe, J. M., Jayne, J. T., Sedlacek, A., Setyan, A., Springston, S., Worsnop,

- D. R., and Zhang, Q.: Enhanced SOA formation from mixed anthropogenic and biogenic emissions during the CARES campaign, *Atmos. Chem. Phys.*, 13, 4, 2091-2113, 2013, 10.5194/acp-13-2091-2013.
- Shilling, J. E., Fortner, E., Pekour, M. S., Artaxo, P., Hubbe, J. M., Longo, K. M., Machado, L. A. T., Martin, S. T., Mei, F., Springston, S. R., Tomlinson, J., and Wang, J.: Particle-phase chemical composition measurements onboard the G-1 research aircraft during the GoAmazon2014/5 campaign in preparation.
- Shrivastava, M., Cappa, C. D., Fan, J., Goldstein, A. H., Guenther, A. B., Jimenez, J. L., Kuang, C., Laskin, A., Martin, S. T., Ng, N. L., Petaja, T., Pierce, J. R., Rasch, P. J., Roldin, P., Seinfeld, J. H., Shilling, J., Smith, J. N., Thornton, J. A., Volkamer, R., Wang, J., Worsnop, D. R., Zaveri, R. A., Zelenyuk, A., and Zhang, Q.: Recent advances in understanding secondary organic aerosol: Implications for global climate forcing, *Rev. Geophys.*, 55, 2, 509-559, 2017, 10.1002/2016RG000540.
- Spracklen, D. V., Jimenez, J. L., Carslaw, K. S., Worsnop, D. R., Evans, M. J., Mann, G. W., Zhang, Q., Canagaratna, M. R., Allan, J., Coe, H., McFiggans, G., Rap, A., and Forster, P.: Aerosol mass spectrometer constraint on the global secondary organic aerosol budget, *Atmos. Chem. Phys.*, 11, 23, 12109-12136, 2011, 10.5194/acp-11-12109-2011.
- Subramanian, R., Roden, C. A., Boparai, P., and Bond, T. C.: Yellow beads and missing particles: trouble ahead for filter-based absorption measurements, *Aerosol Sci Technol*, 41, 6, 630-637, 2007, 10.1080/02786820701344589.
- Sueper, D. and collaborators: ToF-AMS Data Analysis Software Webpage, [http://cires1.colorado.edu/jimenez-group/wiki/index.php/ToF-AMS\\_Analysis\\_Software](http://cires1.colorado.edu/jimenez-group/wiki/index.php/ToF-AMS_Analysis_Software), last access: August 2017.
- Surratt, J. D., Chan, A. W., Eddingsaas, N. C., Chan, M., Loza, C. L., Kwan, A. J., Hersey, S. P., Flagan, R. C., Wennberg, P. O., and Seinfeld, J. H.: Reactive intermediates revealed in secondary organic aerosol formation from isoprene, *Proc. Natl. Acad. Sci. USA*, 107, 15, 6640-6645, 2010, 10.1073/pnas.0911114107.
- Thalman, R., de Sá, S. S., Palm, B. B., Barbosa, H. M. J., Pöhlker, M. L., Alexander, M. L., Brito, J., Carbone, S., Castillo, P., Day, D. A., Kuang, C., Manzi, A., Ng, N. L., Sedlacek Iii, A. J., Souza, R., Springston, S., Watson, T., Pöhlker, C., Pöschl, U., Andreae, M. O., Artaxo, P., Jimenez, J. L., Martin, S. T., and Wang, J.: CCN activity and organic hygroscopicity of aerosols downwind of an urban region in central Amazonia: seasonal and diel variations and impact of anthropogenic emissions, *Atmos. Chem. Phys.*, 17, 19, 11779-11801, 2017, 10.5194/acp-17-11779-2017.
- Tsigaridis, K., Krol, M., Dentener, F. J., Balkanski, Y., Lathière, J., Metzger, S., Hauglustaine, D. A., and Kanakidou, M.: Change in global aerosol composition since preindustrial times, *Atmos. Chem. Phys.*, 6, 12, 5143-5162, 2006, 10.5194/acp-6-5143-2006.
- Ulbrich, I., Handschy, A., Lechner, M. J., and Jimenez, J.: High-Resolution AMS Spectral Database, 2009a, <http://cires.colorado.edu/jimenez-group/HRAMSsd/>, last access: August 2017.
- Ulbrich, I., Canagaratna, M., Zhang, Q., Worsnop, D., and Jimenez, J.: Interpretation of organic components from positive matrix factorization of aerosol mass spectrometric data, *Atmos. Chem. Phys.*, 9, 9, 2891-2918, 2009b, 10.5194/acp-9-2891-2009.
- Ulbrich, I., Handschy, A., Lechner, M. J., and Jimenez, J.: AMS Spectral Database, 2009c, <http://cires.colorado.edu/jimenez-group/AMSsd/>, last access: August 2017.



- van Pinxteren, D., Neusüß, C., and Herrmann, H.: On the abundance and source contributions of dicarboxylic acids in size-resolved aerosol particles at continental sites in central Europe, *Atmos. Chem. Phys.*, 14, 8, 3913-3928, 2014.
- Weber, R. J., Sullivan, A. P., Peltier, R. E., Russell, A., Yan, B., Zheng, M., de Gouw, J., Warneke, C., Brock, C., Holloway, J. S., Atlas, E. L., and Edgerton, E.: A study of secondary organic aerosol formation in the anthropogenic-influenced southeastern United States, *J. Geophys. Res. Atmos.*, 112, D13, D13302, 2007, 10.1029/2007JD008408.
- Worton, D. R., Surratt, J. D., LaFranchi, B. W., Chan, A. W. H., Zhao, Y., Weber, R. J., Park, J.-H., Gilman, J. B., de Gouw, J., Park, C., Schade, G., Beaver, M., Clair, J. M. S., Crouse, J., Wennberg, P., Wolfe, G. M., Harrold, S., Thornton, J. A., Farmer, D. K., Docherty, K. S., Cubison, M. J., Jimenez, J.-L., Frossard, A. A., Russell, L. M., Kristensen, K., Glasius, M., Mao, J., Ren, X., Brune, W., Browne, E. C., Pusede, S. E., Cohen, R. C., Seinfeld, J. H., and Goldstein, A. H.: Observational insights into aerosol formation from isoprene, *Environ. Sci. Technol.*, 47, 20, 11403-11413, 2013, 10.1021/es4011064.
- Xu, L., Guo, H., Boyd, C. M., Klein, M., Bougiatioti, A., Cerully, K. M., Hite, J. R., Isaacman-VanWertz, G., Kreisberg, N. M., Knote, C., Olson, K., Koss, A., Goldstein, A. H., Hering, S. V., de Gouw, J., Baumann, K., Lee, S.-H., Nenes, A., Weber, R. J., and Ng, N. L.: Effects of anthropogenic emissions on aerosol formation from isoprene and monoterpenes in the southeastern United States, *Proc. Natl. Acad. Sci. USA*, 112, 1, 37-42, 2015a, 10.1073/pnas.1417609112.
- Xu, L., Suresh, S., Guo, H., Weber, R. J., and Ng, N. L.: Aerosol characterization over the southeastern United States using high-resolution aerosol mass spectrometry: spatial and seasonal variation of aerosol composition and sources with a focus on organic nitrates, *Atmos. Chem. Phys.*, 15, 13, 7307-7336, 2015b, 10.5194/acp-15-7307-2015.
- Yáñez-Serrano, A. M., Nölscher, A. C., Williams, J., Wolff, S., Alves, E., Martins, G. A., Bourtsoukidis, E., Brito, J., Jardine, K., Artaxo, P., and Kesselmeier, J.: Diel and seasonal changes of biogenic volatile organic compounds within and above an Amazonian rainforest, *Atmos. Chem. Phys.*, 15, 6, 3359-3378, 2015, 10.5194/acp-15-3359-2015.
- Zhang, H., Yee, L. D., and Goldstein, A. H.: Monoterpenes are the largest source of summertime organic aerosol in the southeastern United States, 2018.
- Zhang, Q., Alfarra, M. R., Worsnop, D. R., Allan, J. D., Coe, H., Canagaratna, M. R., and Jimenez, J. L.: Deconvolution and quantification of hydrocarbon-like and oxygenated organic aerosols based on aerosol mass spectrometry, *Environ. Sci. Technol.*, 39, 13, 4938-4952, 2005, 10.1021/es048568l.
- Zhang, Q., Jimenez, J. L., Canagaratna, M. R., Ulbrich, I. M., Ng, N. L., Worsnop, D. R., and Sun, Y.: Understanding atmospheric organic aerosols via factor analysis of aerosol mass spectrometry: a review, *Anal. Bioanal. Chem.*, 401, 10, 3045-3067, 2011, 10.1007/s00216-011-5355-y.

## List of Tables

**Table 1.** Characteristics of the PMF factors derived from the AMS datasets. Listed are signal fractions  $f_{\text{CO}_2^+}$  at nominal  $m/z$  44 and oxygen-to-carbon (O:C) and hydrogen-to-carbon (H:C) ratios. Values and associated uncertainties were calculated by running PMF in “bootstrap mode” (Ulbrich et al., 2009b). Elemental ratios were calibrated by the “improved-ambient” method, which has an estimated uncertainty of 12% for O:C and 4% for H:C (Canagaratna et al., 2015).

| PMF factor | $f_{\text{CO}_2^+}$ | O:C             | H:C             |
|------------|---------------------|-----------------|-----------------|
| MO-OOA     | $0.25 \pm 0.01$     | $1.09 \pm 0.17$ | $1.27 \pm 0.12$ |
| LO-OOA     | $0.14 \pm 0.02$     | $0.72 \pm 0.10$ | $1.49 \pm 0.07$ |
| IEPOX-SOA  | $0.17 \pm 0.01$     | $0.93 \pm 0.10$ | $1.39 \pm 0.07$ |
| ADOA       | $0.11 \pm 0.01$     | $0.40 \pm 0.05$ | $1.63 \pm 0.02$ |
| BBOA       | $0.123 \pm 0.004$   | $0.61 \pm 0.08$ | $1.57 \pm 0.04$ |
| HOA        | $0.048 \pm 0.006$   | $0.18 \pm 0.02$ | $1.94 \pm 0.02$ |

**Table 2.** Coordinates of cluster centroids for input variables, AMS species concentrations, and PMF factor loadings. Table entries for AMS species and PMF factors are plotted in Figure 8. The AMS species concentrations (except for sulfate) and PMF factor loadings were not used as input variables in the FCM clustering analysis.

| Species   | Cluster Centroid |        |       |       |
|---|------------------|--------|-------|-------|
|   | Bkgd-1           | Bkgd-2 | Pol-1 | Pol-2 |
| <b>Input variables</b>                                |                  |        |       |       |
| Particle number (cm <sup>-3</sup> )                   | 714              | 1117   | 2636  | 6697  |
| NO <sub>y</sub> (ppb)                                 | 0.64             | 0.95   | 1.2   | 2.2   |
| O <sub>3</sub> (ppb)                                  | 14               | 17     | 26    | 36    |
| Black carbon (μg m <sup>-3</sup> )                    | 0.05             | 0.16   | 0.21  | 0.18  |
| Sulfate (μg m <sup>-3</sup> )                         | 0.15             | 0.36   | 0.44  | 0.57  |
| <b>AMS species concentrations (μg m<sup>-3</sup>)</b> |                  |        |       |       |
| Organic   | 0.96             | 2.0    | 2.5   | 2.6   |
| Ammonium  | 0.05             | 0.12   | 0.15  | 0.21  |
| Nitrate   | 0.03             | 0.07   | 0.10  | 0.12  |
| Chloride  | 0.007            | 0.011  | 0.009 | 0.007 |
| <b>PMF factor loadings (μg m<sup>-3</sup>)</b>        |                  |        |       |       |
| MO-OOA  | 0.29             | 0.83   | 1.13  | 1.13  |
| LO-OOA  | 0.38             | 0.41   | 0.62  | 0.77  |
| IEPOX-SOA   | 0.18             | 0.49   | 0.43  | 0.29  |
| ADOA  | 0.044            | 0.086  | 0.19  | 0.32  |
| BBOA  | 0.028            | 0.054  | 0.081 | 0.063 |
| HOA   | 0.017            | 0.027  | 0.039 | 0.040 |

## List of Figures

**Figure 1.** (a) Mass concentrations of PM<sub>1</sub> species at T3 during the wet season of 2014 (IOP1).

Non-refractory (NR) PM<sub>1</sub> species of organic, sulfate, ammonium, nitrate, and chloride were measured by the AMS. Mass concentrations of black carbon were obtained by scaling aethalometer measurements by a factor of 2 based on the range of 1 to 3 for the comparison of SP2 to aethalometer measurements. The temporal trend of the two instruments agreed well. (b) Comparison of the summed mass concentrations of non-refractory PM<sub>1</sub> species (top) and the mass fractions of these species (bottom) at T3 and three other regional sites. T0a-2015 refers to measurements in the wet season of 2015 at the ATTO location (Andreae et al., 2015). T0t-2008 refers to the AMAZE-08 experiment, which took place in the wet season of 2008 at the TT34 location (Chen et al., 2015). T2-2014 refers to measurements made during IOP1 at a site 8 km downwind of Manaus, just across the Black River ("Rio Negro) (Cirino et al., submitted). Measurements at T0a in 2015 and at T2 in 2014 were made by an ACSM, and measurements at T0t in 2008 and at T3 in 2014 were made by an AMS. Concentrations were adjusted to standard temperature (273.15 K) and pressure (10<sup>5</sup> Pa). The variability of measurements across sites is evaluated in Figure 2.

**Figure 2.** Diel patterns of the mass concentrations of organic (top, green) and sulfate (bottom, red) species during the wet season at four different sites (cf. Fig. 1 and Fig. S1). The ordinate scale for the T2-2014 panel is twice that of the other panels. Mass concentrations were corrected to standard temperature and pressure (273.15 K and 10<sup>5</sup> Pa). Local time is (UTC - 4 h). Lines represent means, solid markers show medians, and boxes span interquartile ranges.

**Figure 3.** Scatter plot of the AMS signal fraction at  $m/z$  44 ( $f_{44}$ ) against that at  $m/z$  43 ( $f_{43}$ ). Gray and blue circles correspond, respectively, to measurements at T3 and T2 during IOP1, in the wet season of 2014. For visualization purposes, the two datasets are plotted separately in panels a and b. Solid squares represent median values, and whiskers represent 10 and 90 percentiles. Dashed lines delineate the region where worldwide measurements of ambient organic  $PM_{10}$  commonly lie (Ng et al., 2011a).

**Figure 4.** Results of the PMF analysis on the time series of AMS organic mass spectra collected at T3. (a) Mass spectral profile of each factor represented at unit mass resolution. The inset shows the mean fractional loading of each factor. (b) Diel trends for the loadings of each PMF factor. Local time is (UTC - 4 h). Lines represent means, solid markers show medians, and boxes span interquartile ranges. (c) Time series of the factor loadings (left axis) and other related measurements at T3 (right axis). Methyl-butyl-tricarboxylic acid is abbreviated as MBTCA.

**Figure 5.** Column plot of Pearson  $R$  correlations between the loading of each PMF factor and values of selected measurements at T3. Abbreviations include tricarballic acid (TCA), methyl-butyl-tricarboxylic acid (MBTCA), methyl vinyl ketone (MVK), methacrolein (MACR), and isoprene hydroxyhydroperoxides (ISOPOOH). SV-TAG measurements refer to particle-phase concentrations. Isomers could not be distinguished by PTR-ToF-MS measurements;  $C_8$  and  $C_9$  aromatics include the xylene and trimethylbenzene isomers, respectively.

**Figure 6.** Results of the cluster analysis by Fuzzy c-means (FCM) for afternoon periods (12:00 to 16:00 h) are presented by several case studies. (a) Degree of membership in each of the four clusters. The sum of degrees of membership across all clusters is unity.

Background conditions are abbreviated as “Bkgd”, and polluted conditions are abbreviated as “Pol”. (b) Pollution indicators: concentrations of  $\text{NO}_y$ ,  $\text{O}_3$ , black carbon (BC), and particle number count are plotted. (c)  $\text{PM}_{10}$  mass concentrations for organic, sulfate, nitrate, and ammonium species. (d) Fractional contribution of each factor to total organic  $\text{PM}_{10}$ .

**Figure 7.** Air mass backtrajectories associated with the four clusters of the FCM analysis for the case studies of Figure 6. Trajectories were calculated using HYSPLIT 4 in steps of 12 min for ten hours (Draxler and Hess, 1998). Image data: Google earth.

**Figure 8.** Characteristic PM composition of the FCM clusters as represented by coordinates of cluster centroids. (a) Mass concentrations of AMS species characteristic of each cluster. (b) PMF factor loadings characteristic of each cluster. Calculations are presented in more detail in the Supplementary Material (Section S3). Values plotted are shown in Table 2.

**Figure 9.** Schematic representation of (a) atmospheric processes, illustrated in a simplified manner, associated with the production of organic  $\text{PM}_{10}$  and (b) observables of these processes as captured by the datasets and analytical approach employed in this study. In panel (a), the left side depicts the emissions of biogenic volatile organic compounds (VOCs), their atmospheric oxidation, and the production of biogenic secondary organic  $\text{PM}_{10}$ . The right side depicts anthropogenic emissions of gas species and particulate matter that can alter natural atmospheric concentrations and processes. There are primary organic  $\text{PM}_{10}$  emissions from traffic, cooking, and industrial activities. Anthropogenic VOCs can be precursors for the production of secondary organic  $\text{PM}_{10}$  and can affect the production of ozone and hydroxyl radical.  $\text{NO}_x$

emissions directly and indirectly alter the natural pathways of PM<sub>1</sub> production in the atmosphere. NO<sub>x</sub> and SO<sub>x</sub> can also directly contribute to the formation of secondary inorganic PM<sub>1</sub> (not shown), which can in turn play a role in changing pathways of secondary organic PM<sub>1</sub> production. In panel (b), different PMF factors represent distinct sources and/or processes. The IEPOX-SOA factor is at the intersection of the two, as it represents both a source (i.e., isoprene emissions from the forest) and a process (i.e., photo-oxidation under HO<sub>2</sub> dominant conditions, influenced by sulfate concentrations). The dashed black line represents the natural and anthropogenic oxidative processes that transform the chemical signature of the HOA, ADOA, BBOA, IEPOX-SOA, and LO-OOA factors after sufficient atmospheric residence time into the MO-OOA factor. The clusters represent different conditions at the receptor site (i.e., T3) and therefore incorporate the meteorological and geographical histories of the air masses that reach the site and affect the observed concentrations. The different PMF factors are associated to the different clusters (solid lines) to various extents (not detailed here for simplification purposes; cf. Figure 8).

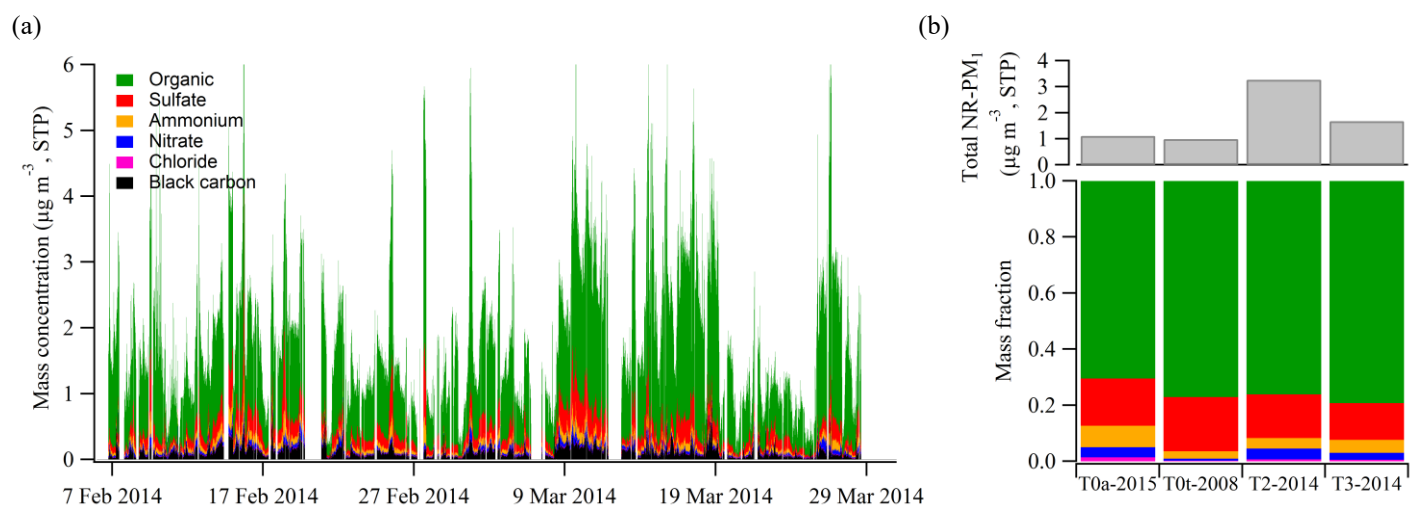


Figure 1



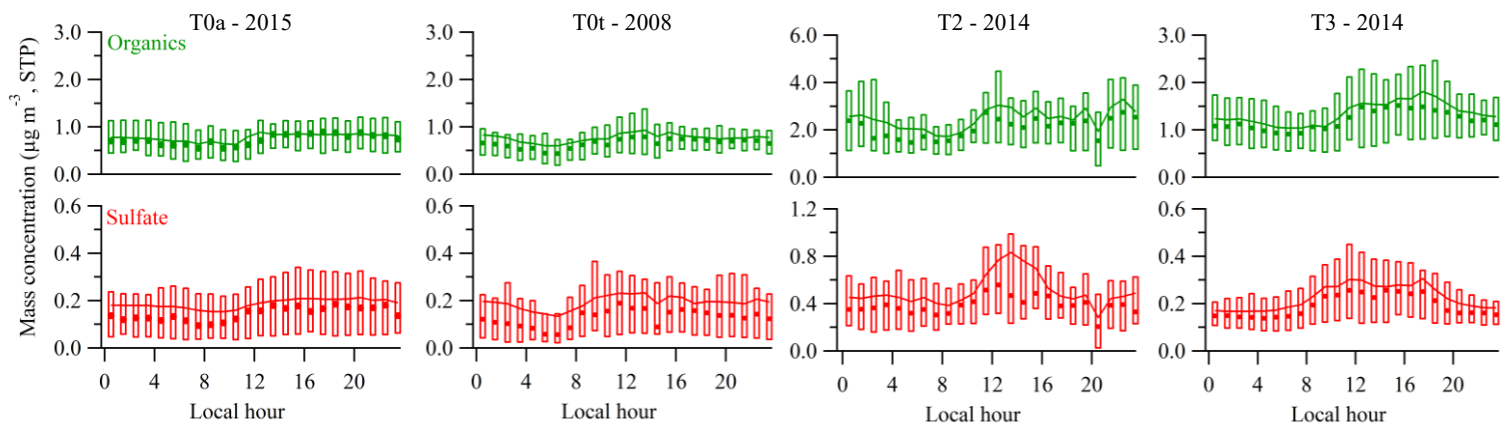


Figure 2

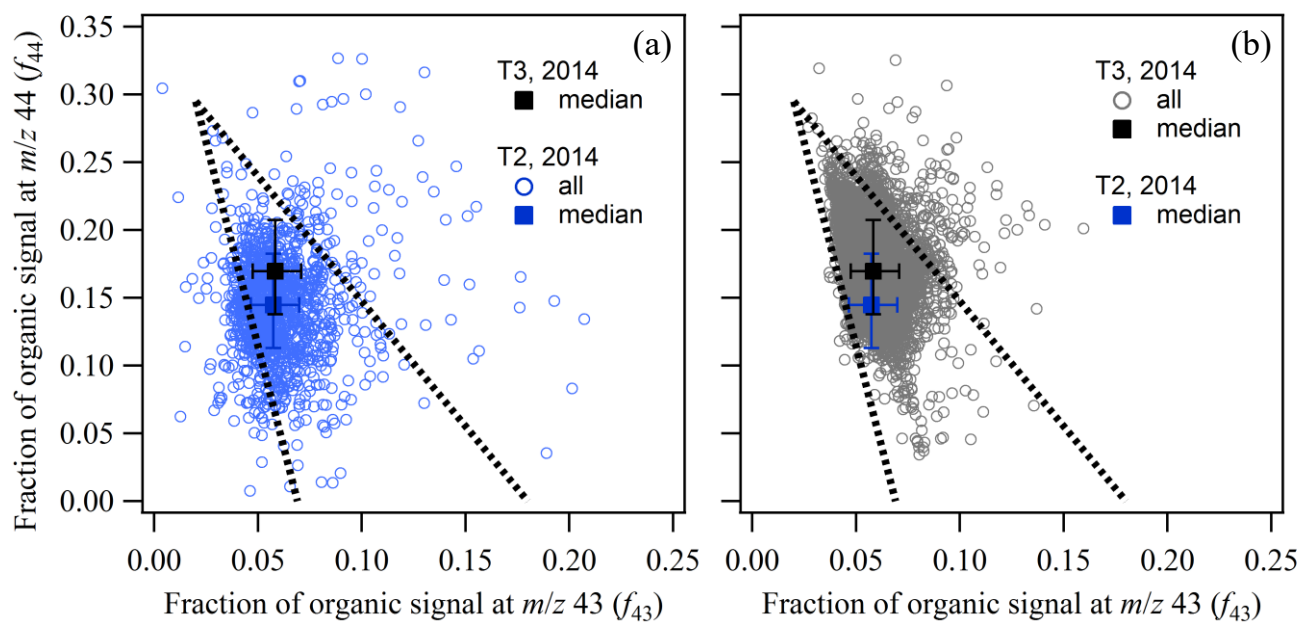


Figure 3

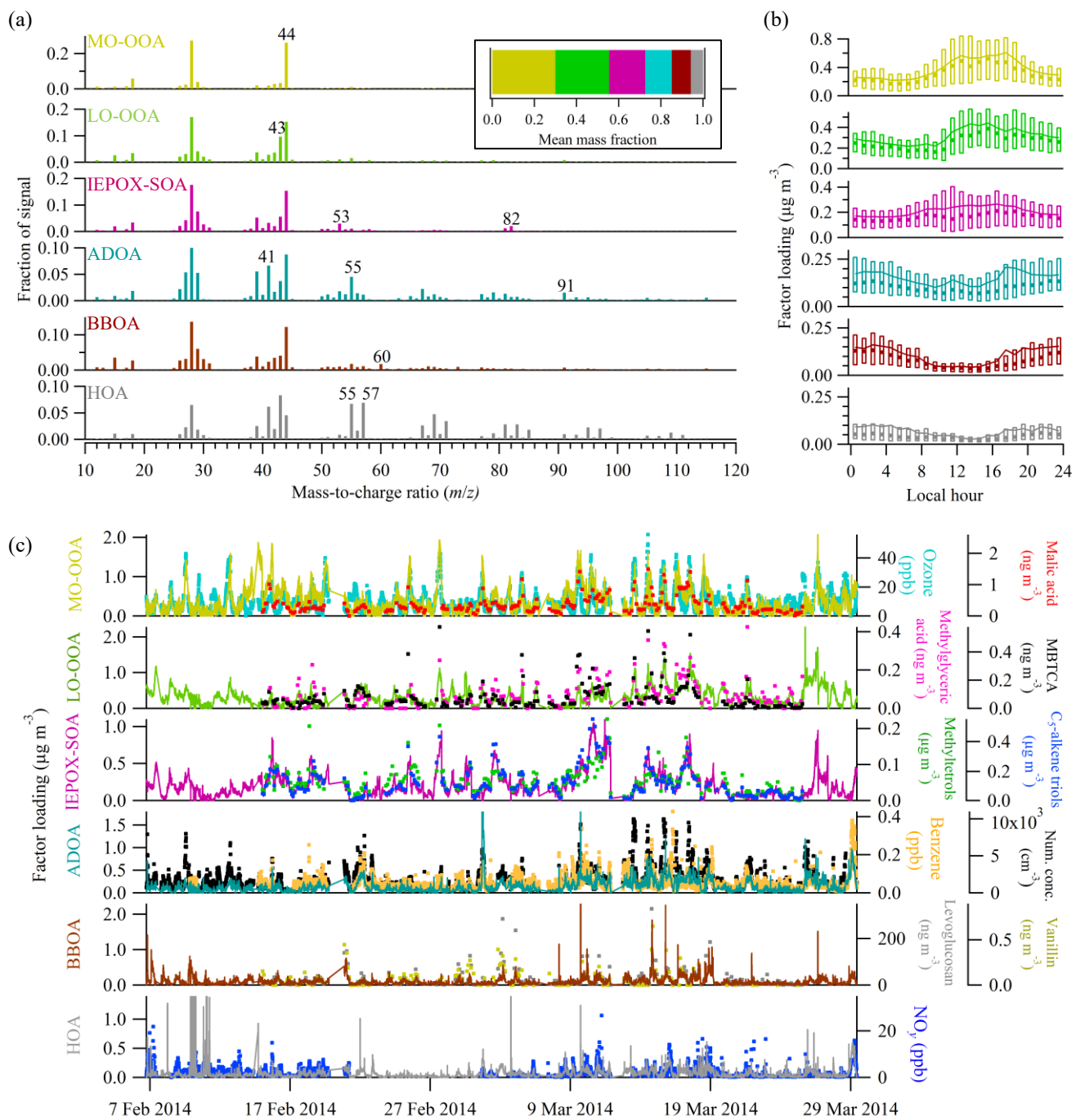


Figure 4

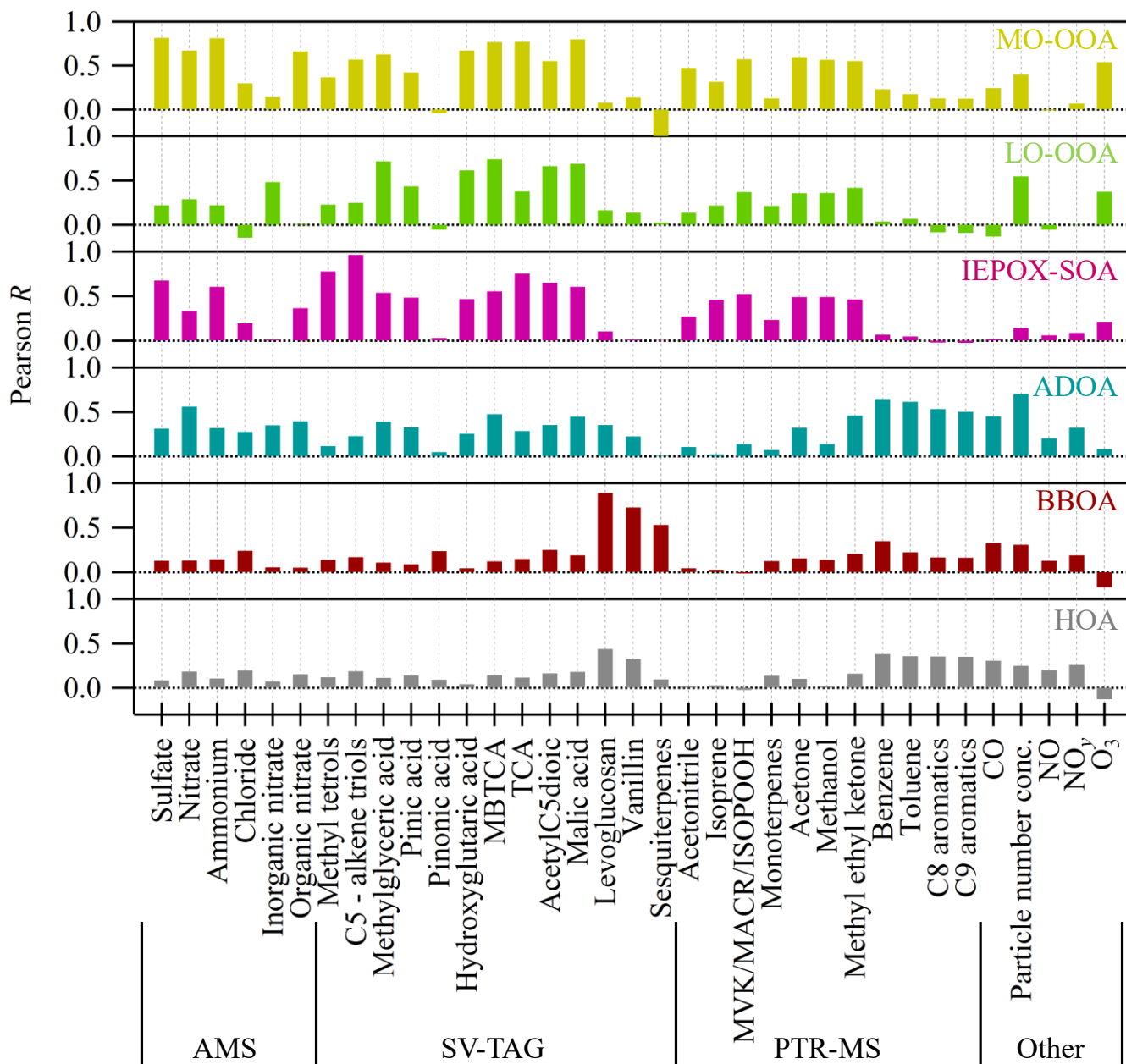


Figure 5

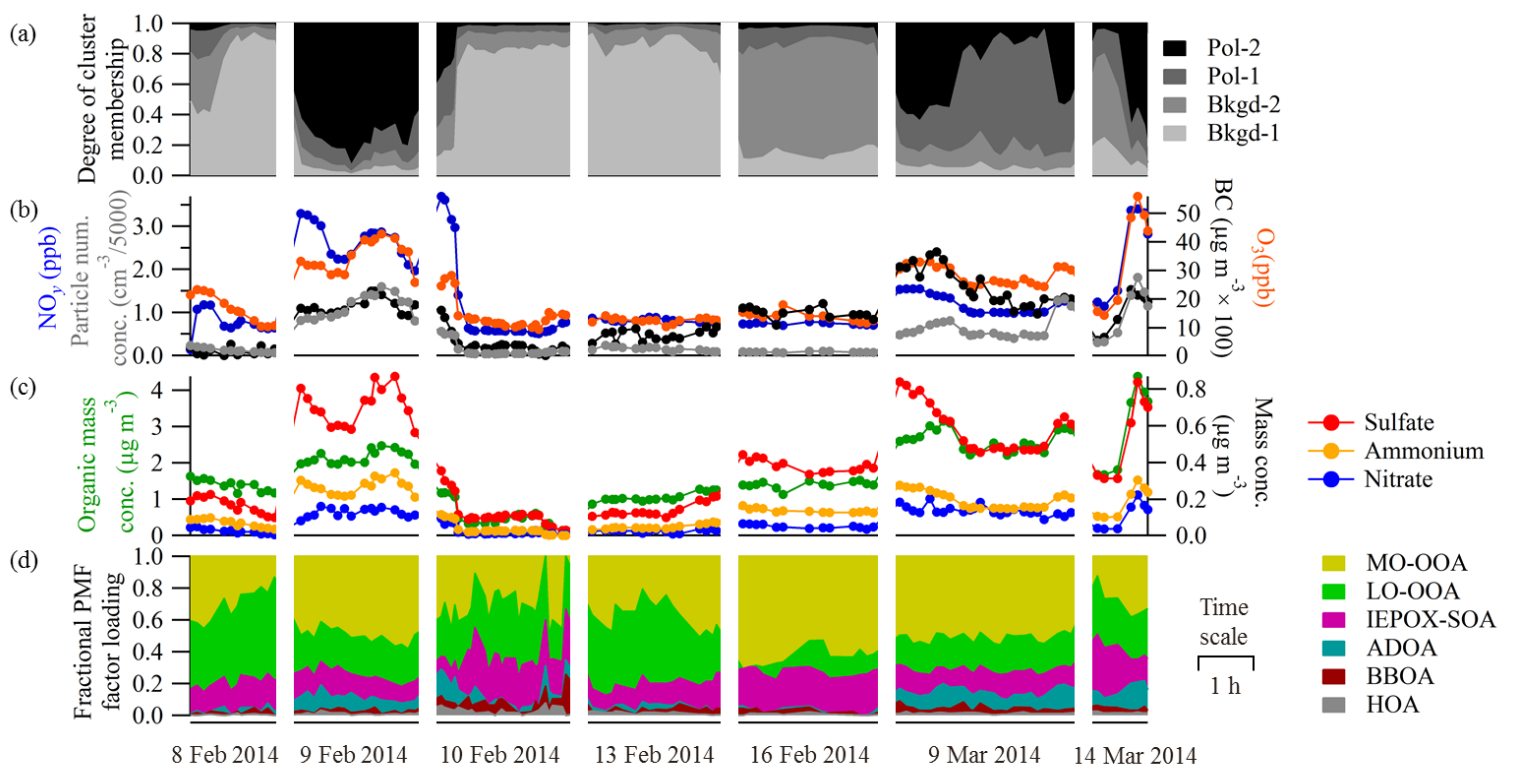


Figure 6

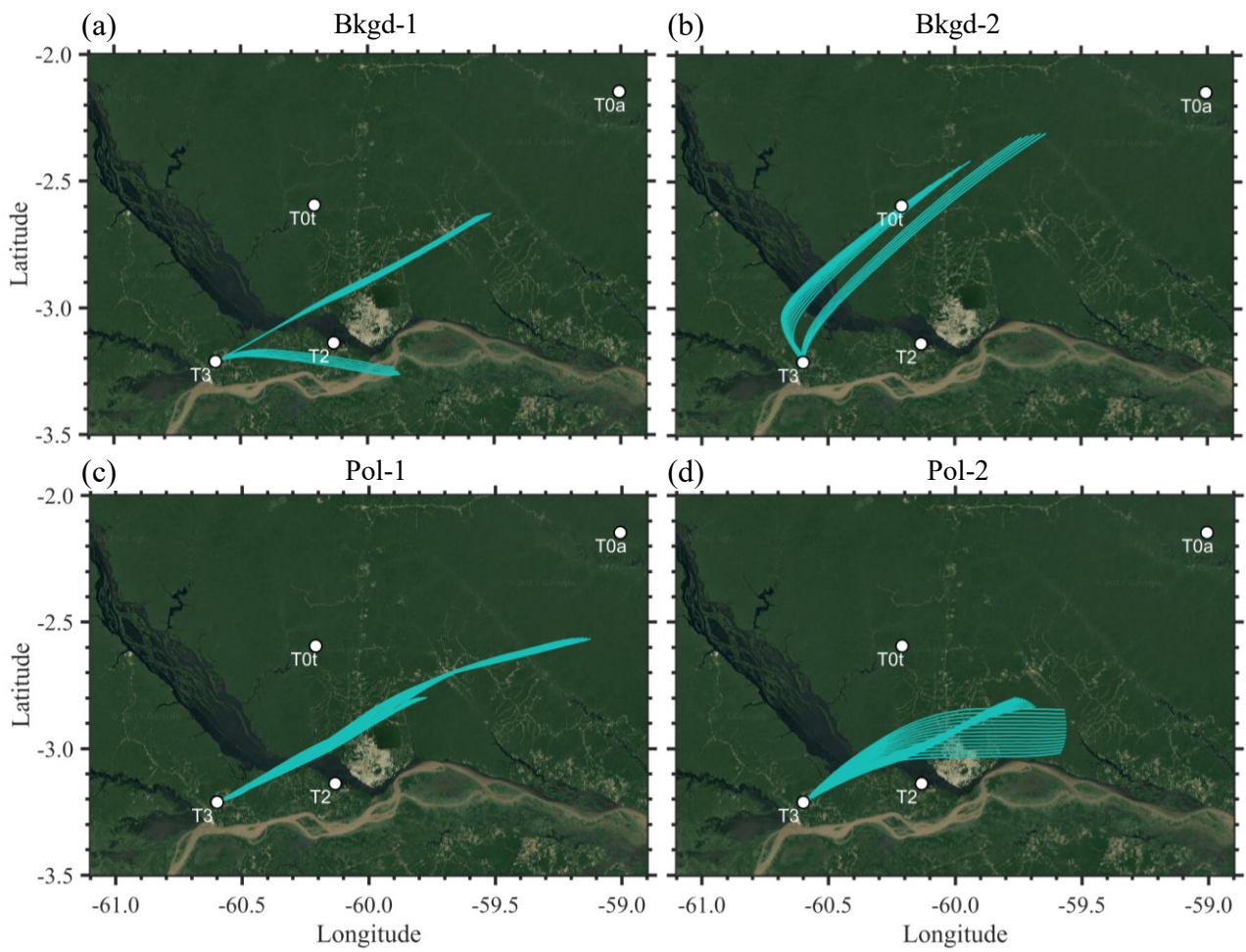


Figure 7

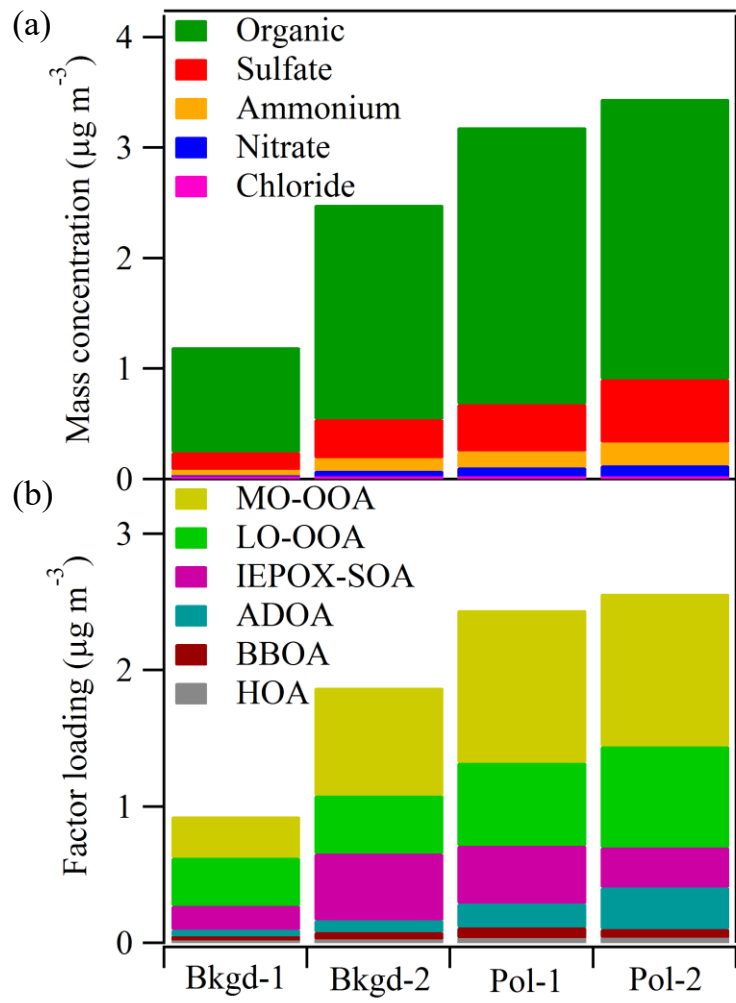


Figure 8

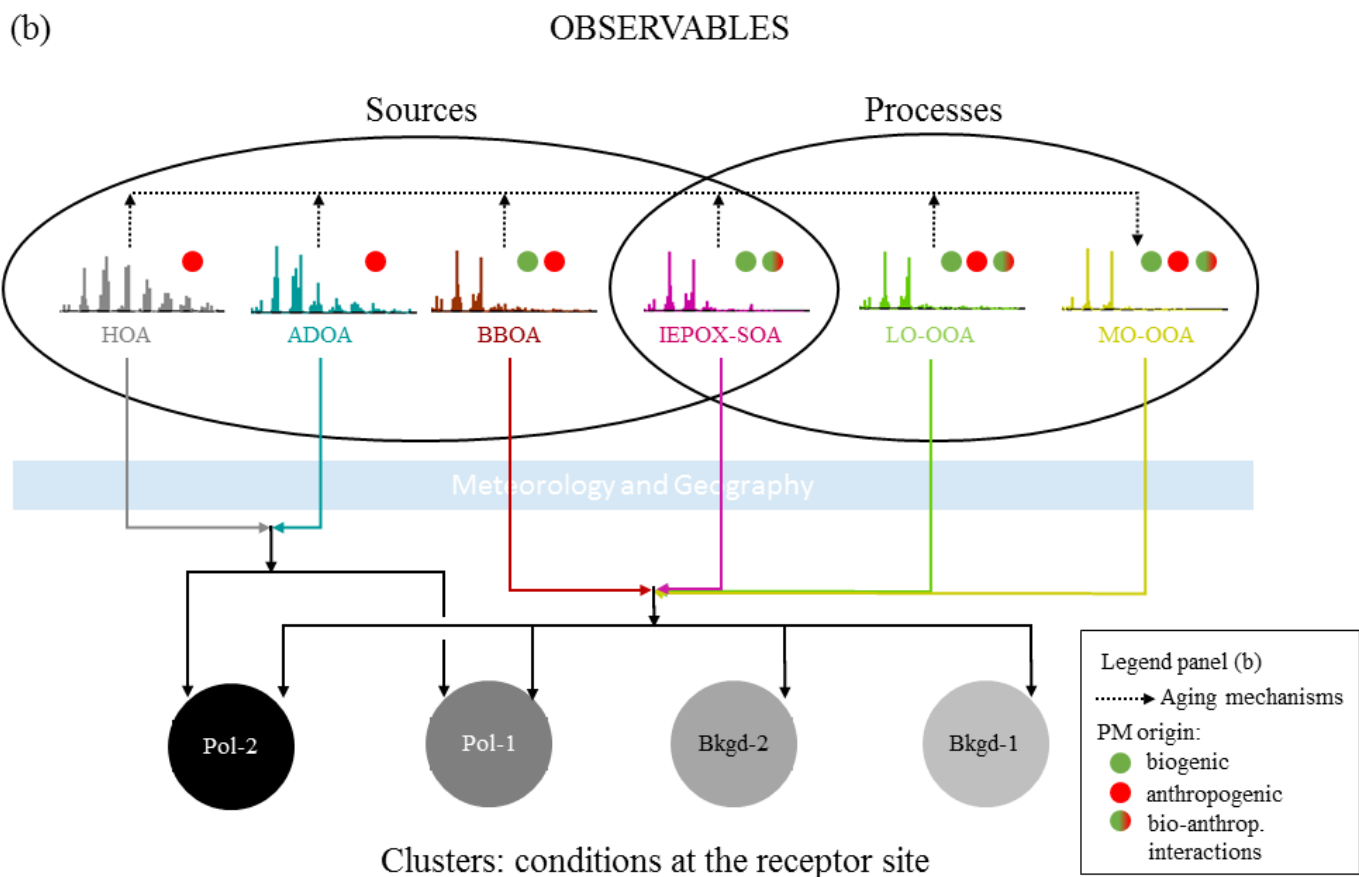
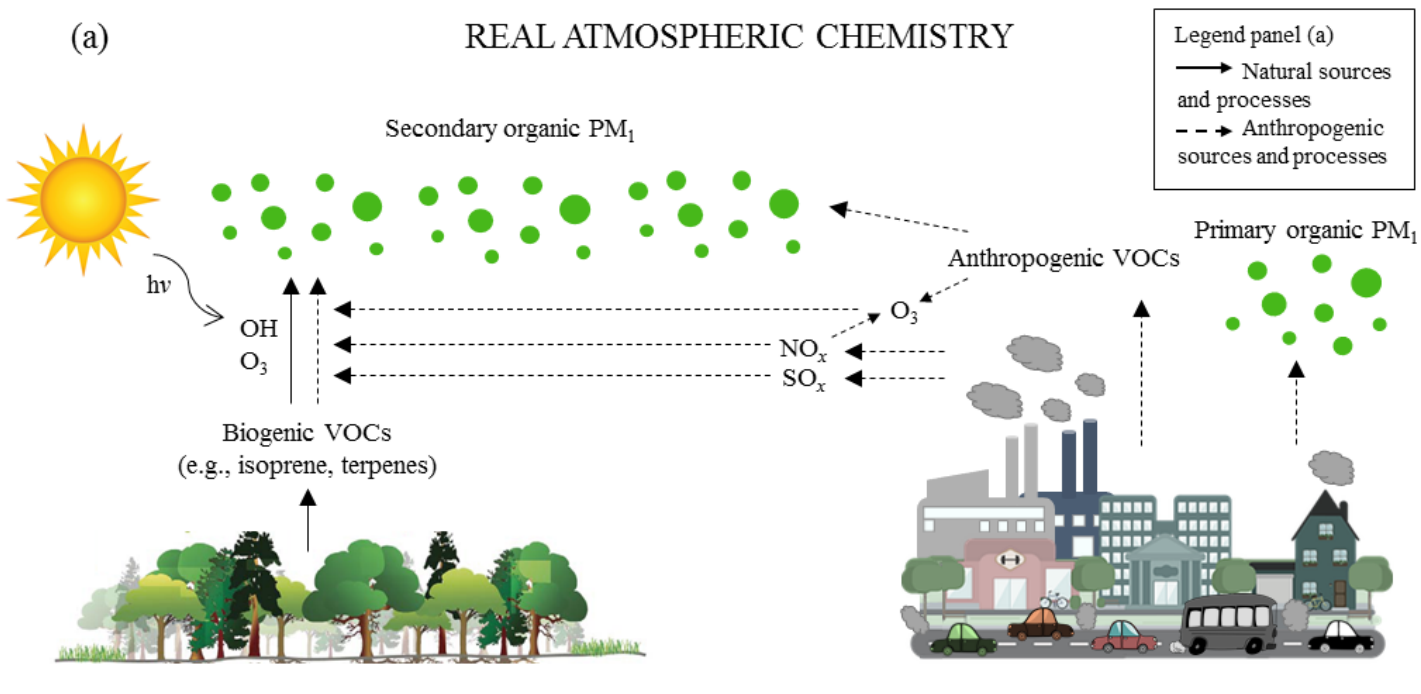


Figure 9